

1

2 **Main Manuscript for**

3 Climate change facilitated the early colonization of the Azores
4 Archipelago during Medieval times.

5

6 Pedro M. Raposeiro^{a,b*}, Armand Hernández^c, Sergi Pla-Rabes^d, Vítor Gonçalves^{a,b}, Roberto Bao^e,
7 Alberto Sáez^f, Timothy Shanahan^g, Mario Benavente^c, Erik J. de Boer^f, Nora Richter^{h,i}, Verónica
8 Gordonⁱ, Helena Marques^{a,b}, Pedro M. Sousa^{j,k}, Martín Souto^{a,b}, Miguel G. Matias^{l,m}, Nicole
9 Aguiar^b, Cátia Pereira^{l,m}, Catarina Ritter^{a,b}, María Jesús Rubio^c, Marina Salcedo^b, David Vázquez-
10 Loureiro^e, Olga Margalef^{d,f}, Linda A. Amaral-Zettler^{h,i,n}, Ana Cristina Costa^{a,b}, Yongsong Huangⁱ,
11 Jacqueline FN van Leeuwen^o, Pere Masqué^{p,q,r}, Ricardo Prego^s, Ana Carolina Ruiz-Fernández^t,
12 Joan-Albert Sánchez-Cabeza^t, Ricardo Trigo^k, and Santiago Giralt^c

13

14 ^a CIBIO, Centro de Investigação em Biodiversidade e Recursos Genéticos, InBIO Laboratório
15 Associado, Pólo dos Açores, Rua da Mãe de Deus, 9500-321 Ponta Delgada, Portugal

16 ^b Faculdade de Ciências e Tecnologia, Universidade dos Açores, Rua da Mãe de Deus, 9500-
17 321 Ponta Delgada, Portugal

18 ^c Geosciences Barcelona (Geo3BCN-CSIC), Lluís Solé i Sabarís s/n, 08028 Barcelona, Spain

19 ^d CREAM, Campus de Bellaterra (UAB), Edifici C, 08193, Cerdanyola del Valles, Spain

20 ^e Centro de Investigacións Científicas Avanzadas (CICA), Facultade de Ciencias, Campus da
21 Zapateira s/n, Universidade da Coruña, 15071 A Coruña, Spain

22 ^f Department de Dinàmica de la Terra i de l'Oceà, Facultat de Ciències de la Terra, Universitat de
23 Barcelona, Martí i Franquès s/n, 08028 Barcelona, Spain

24 ^g Department of Geosciences, University of Texas at Austin, Austin, TX 78712, USA

25 ^h NIOZ Royal Netherlands Institute for Sea Research, P.O. Box 59, 1790 AB Den Burg, The
26 Netherlands

27 ⁱ Department of Earth, Environmental and Planetary Sciences, Brown University, Providence, RI
28 02912, USA

29 ^j Instituto Português do Mar e da Atmosfera (IPMA), 1749-077 Lisboa, Portugal

30 ^k Instituto Dom Luiz (IDL), Faculdade de Ciências, Universidade de Lisboa, 1749-016 Lisbon,
31 Portugal

32 ^l Departamento de Biogeografía y Cambio Global, Museo Nacional de Ciencias Naturales, CSIC,
33 Madrid, Spain

34 ^m Biodiversity Research Chair - MED – Mediterranean Institute for Agriculture, Environment and
35 Development. Universidade de Évora, Rua Dr. Joaquim Henrique da Fonseca. Casa do Cordovil,
36 N^o7, 2^o Andar. 7000-890, Évora, Portugal

37 ⁿ Department of Freshwater and Marine Ecology, Institute for Biodiversity and Ecosystem
38 Dynamics, University of Amsterdam, The Netherlands

39 ^o Institute of Plant Sciences and Oeschger Center for Climate Change Research, University of
40 Bern, Switzerland

41 ^p International Atomic Energy Agency, 4a Quai Antoine 1er, 98000 Principality of Monaco,
42 Monaco

43 ^q Institute of Environmental Science and Technology (ICTA) and Physics Department, Universitat
44 Autònoma de Barcelona, Bellaterra, 08193, Spain

45 ^r School of Natural Sciences, Centre for Marine Ecosystems Research, Edith Cowan University,
46 Joondalup, WA 6027, Australia

47 ^s Department of Oceanography, Marine Research Institute (CSIC), 36208 Vigo, Spain

48 ^t Universidad Nacional Autónoma de México, Instituto de Ciencias del Mar y Limnología, Unidad
49 Académica Mazatlán, Calz. J. Montes Camarena s/n, 82040 Mazatlán, Mexico

50 *Pedro M. Raposeiro

51 **Email:** pedro.mv.raposeiro@uac.pt

52 **Author Contributions:** PMR, AH, SP, VG, RB, AS, SG designed research; PMR, AH, SP, VG,
53 RB, AS, TS, MB, EB, HM, PS, MS, MM, NA, CP, CR, MS, NR, LAA-Z, MJR, DV, ACC, VG, YH,
54 JFNL, PM, RP, ACRF, JASC, OM, RT, SG performed research and contributed raw data; PMR,
55 AH, SP, VG, RB, AS, PS, SG analyzed data; PMR, AH, SP, VG, RB, AS, TS SG wrote the paper;
56 all authors revised the first draft and accepted the final version.

57 **Competing Interest Statement:** Disclose any competing interests here.

58 **Classification:** Paste the major and minor classification here. Dual classifications are permitted,
59 but cannot be within the same major classification.

60 **Keywords:** Paleolimnology | island colonization | biomarkers | climate simulations | ecosystem
61 disruption |.

62

63 **This PDF file includes:**

64 Main Text

65 Figures 1 to 4

66

67 **Abstract**

68 Humans have made such dramatic and permanent changes to Earth's landscapes that much of it
69 is now substantially and irreversibly altered from its pre-anthropogenic state. Remote islands,
70 until recently isolated from humans, offer insights into how these landscapes evolved in response
71 to human-induced perturbations. However, little is known about when and how remote systems
72 were colonized because archaeological data and historical records are scarce and incomplete.
73 Here we use a multi-proxy approach to reconstruct the initial colonization and subsequent
74 environmental impacts on the Azores Archipelago. Our reconstructions provide unambiguous
75 evidence for widespread human disturbance of this archipelago starting between 700.₋₆₀⁺⁵⁰ and
76 850.₋₆₀⁺⁶⁰ CE, ca. 700 years earlier than historical records suggest the onset of Portuguese
77 settlement of the islands. Settlement proceeded in three phases, during which human pressure
78 on the terrestrial and aquatic ecosystems grew steadily (i.e., through livestock introductions,
79 logging and fire), resulting in irreversible changes. Our climate models suggest that the initial
80 colonization at the end of the Early Middle Ages (500 – 900 CE) occurred in conjunction with
81 anomalous northeasterly winds and warmer Northern Hemisphere temperatures. These climate
82 conditions likely inhibited exploration from southern Europe and facilitated human settlers from
83 the northeast Atlantic. These results are consistent with recent archaeological and genetic data
84 suggesting that the Norse were most likely the earliest settlers on the islands.

85 **Significance Statement**

86 We use a diverse set of lake and landscape proxy indicators to characterize initial human
87 occupation and its impacts on the Azores Archipelago. The occupation of these islands began
88 between 700 and 850 CE, 700 years earlier than suggested by official documentary sources.
89 These early occupations caused widespread ecological and landscape disturbance, and raise
90 doubts about the islands' presumed pristine nature during Portuguese arrival. The earliest
91 explorers arrived at the end of the Early Middle Ages, when temperatures were higher-than-
92 average, and the westerly winds were weaker, facilitating arrivals to the archipelago from
93 northeastern Europe and inhibiting exploration from southern Europe. This is consistent with
94 recent archaeological and genetic research suggesting the Norse were the first to colonize the
95 Azores Archipelago.

96

97 **Introduction**

98 The Azores Archipelago (36.5°- 40°N – 24.5°- 31.5°W) is made up of nine volcanic islands in the
99 North Atlantic (Fig.1), and given their distance from the European coast (ca. 1450 km), the
100 colonization of these islands would not have been possible after the advent of ocean-worthy ships
101 (1). Until recently, the consensus has been that the Azores were not colonized until the
102 Portuguese arrived between 1427 CE (Santa Maria Island) and 1452 CE (Flores and Corvo
103 Islands) (2–5) while searching for new routes to Asia (6). Historical documents from the first
104 settlers note the apparent pristine and undisturbed character of the islands (2, 3, 7). However, the
105 presence of the Azores archipelago on maps such as those of Pizzigani (1367 CE), the Medici-
106 Laurentian (1370 CE), the Catalan (1375 CE), the Pinelli–Walckenaer (1384 CE), the Corbitis (c.
107 1385–1410 CE) Atlas, as well as their listing in the Libro del Conoscimiento (c. 1380 CE),
108 suggests that these remote islands were well-known before their official settlement recorded in
109 Portuguese historical documents. This, raises questions both about the timing of the first human
110 arrivals to the islands and the pristine nature of these systems at that time.

111 To improve our understanding of the early colonization history and subsequent environmental
112 impacts of early settlers on the Azores, we studied sediment cores from lakes on five islands in
113 the Archipelago (Fig.1): Lake Caldeirão (Corvo Island; 39.7023° N - 31.1080° W; 400 m asl),
114 Lake Funda (Flores Island; 39.4475° N - 31.1939° W; 360 m asl), Lake Peixinho (Pico Island;
115 38.4580° N - 28.3228° W; 870 m asl), Lake Ginjal (Terceira Island; 38.7216° N - 27.2206° W; 390
116 m asl), and Lake Azul (São Miguel Island; 37.7804° N - 25.4970° W; 260 m asl). Age models for
117 each of the records were generated using a combination of ²¹⁰Pb, ¹³⁷Cs, and radiocarbon dating
118 (see Methods). The records vary in length, with the shortest records extending back to ~600 yr
119 cal. BP (Azul, Ginjal), while others cover the last ~1000 yr cal. BP (Funda), ~2700 yr cal. BP
120 (Peixinho) and the longest to ~3800 yr cal. BP (Caldeirão). Only the last two cover the time range
121 hypothesized for the Norse arrival in the Azores but all records cover at least the last six hundred
122 years of historical human occupation. Collectively, these records provide integrative and novel
123 insights into the human settlement process and its environmental impacts across five different
124 islands that span 600 km along a range of physiographic settings (i.e., altitude, area, orography,
125 and hydrology) in the North Atlantic Ocean.

126 Lake sediments can provide robust, continuous, and high-resolution archives of environmental
127 changes (8). Disentangling the effects of climate change and anthropogenic activities on the
128 environment is, however, a major challenge because the signal of past anthropogenic activity is
129 often difficult to differentiate from the impacts of climate variability. To overcome this challenge,
130 we use faecal sterol biomarkers, coprostanol (5 β -cholestan-3 β -ol) and 5 β -stigmastanol, as well
131 as coprophilous fungal spores (*Sporormiella*-type, *Sordaria*-type and *Podospora*-type; see
132 Methods) to identify human activities, related to the introduction of large herbivorous mammals
133 (i.e., livestock) (9). Sterols are abundant in mammal faeces, and coprostanol is particularly
134 abundant (~60%) in human faeces and other omnivores (10, 11). We cannot use coprostanol to
135 distinguish between humans and other omnivores, therefore we use coprostanol as an indicator
136 of human activities. In contrast, faeces from ruminants, such as cows and sheep, contain
137 proportionally higher concentrations of 5 β -stigmastanol (11, 12). Coprophilous fungi life cycles
138 depend on herbivorous mammals as they ingest the spores during feeding and then are released
139 in the dung where the fungi grow and sporulate (13). Thus, spores from coprophilous fungi are
140 proxies for larger herbivores, which were not present on the Azores before humans introduced
141 livestock (14, 15). Together, these proxies provide unequivocal evidence for the presence of
142 humans and the introduction of ruminants to these oceanic islands. Since the earliest arrivals
143 may not have had sufficient human or ruminant population densities to leave a significant imprint
144 on lake records, we interpret this proxy as providing a minimum age for human arrival.

145 In addition to faecal sterols, and to assess the role of human settlement on landscape
146 degradation and ecological disruption, we also used a complementary set of proxy-based
147 indicators to simultaneously investigate human impacts on terrestrial and aquatic environments.
148 Variations in pollen, plant macrofossil, charcoal particles, and polycyclic aromatic hydrocarbons
149 (PAH) provide indicators of past vegetation change and fire disturbance (8, 16, 17). In addition,
150 major and trace element variations were used to assess changes in soil erosion (18). Similarly,
151 bulk and isotopic measurements of organic carbon and nitrogen reflect changes in terrestrial and
152 aquatic inputs (18). Distributions of fossil diatoms and chironomids were used as indicators of
153 ecological changes in the lake and catchment ecosystems (19, 20). Finally, to better understand
154 the climate conditions under which the early colonization of the Archipelago occurred (850 CE),
155 we use outputs from the Community Earth System Model (CESM-CAM5_CN) Last Millennium
156 Ensemble (LME) transient simulation (21).

157 Although ecological indicators of disturbance can be impacted by both anthropogenic and natural
158 drivers, we argue that the changes observed in our records are distinctly different than the
159 response to natural forcings. In records from Lake Caveiro (Pico island) and Lake Rasa (Flores
160 island) that span the mid-Holocene (~6000 yr and ~3000 yr long, respectively), episodic
161 increases in fire occur, presumably as a result of lightning ignition, or volcanic eruptions (22).
162 However, the terrestrial and aquatic ecosystem response to these events, reconstructed through
163 pollen and diatom proxies, is generally small, or in the case of eruptions, where impacts can be
164 significant, the recovery is relatively rapid (22, 23). By contrast, the alteration of natural drivers
165 had lasting impacts, mainly because native forests had little history of fire and little resilience to
166 the intensity of burning. This longer-term context for ecosystem variability demonstrates the
167 relative resilience of these oceanic island systems to natural climate change and highlights the
168 distinct impacts of human influences.

169 **Results and Discussion**

170 Using faecal biomarkers, we identified four phases related to the presence of human activity in
171 the sediment core records (Fig.2). During Phase I (500-700 CE), human activities are not
172 detected in any of the records. Phase II is defined by the first appearance of 5 β -stigmastanol
173 between 700-1070 CE. Phase III is defined by the first appearance of coprostanol in the sediment
174 record after 1070 CE, and notable changes within the catchment areas, including increased fire
175 activity and soil erosion. Finally, coinciding with the official Portuguese arrival to the archipelago
176 (1427-1452 CE), Phase IV is defined by additional changes in the proxy records, such as a
177 decline in forested areas and lake eutrophication, that are still visible in the present-day
178 landscape.

179 The lack of faecal biomarkers during Phase I, suggests that humans and ruminants were absent
180 in the lake catchments areas before ~700 CE. Like most of the oceanic islands of Macaronesia,
181 except for the Canary Islands, the Azores Archipelago was devoid of non-volant mammals and
182 larger birds prior to the arrival of humans (15, 24). Pyrolytic PAHs and macrocharcoal display
183 relatively stable and low background levels during this period (accumulation rates of 1.34 ± 109
184 $\mu\text{g cm}^{-2} \text{y}^{-1}$; 0.3 ± 0.1 particles $\text{cm}^{-2} \text{y}^{-1}$, respectively), reflecting the low frequency of natural fires
185 in the lake catchments. Furthermore, the plant macrofossils and pollen data indicate that the
186 islands were densely forested with *Juniperus brevifolia* and *Ilex perado* in co-dominance with
187 *Myrsine africana* shrubs and mosses, which cover branches of trees and shrubs in this
188 environment (see *SI Appendix*, Fig. S1 – S6 and (25–27)). The maritime climate of the islands
189 would have contributed to a stable forest composition (23, 26). Environmental conditions within
190 the lake systems were also relatively stable, with lake organic matter dominated by allochthonous
191 sources and diatom communities of mostly oligo/mesotrophic taxa, indicating stable and relatively
192 low aquatic productivity (*SI Appendix*, Fig. S1 – S5 and Fig. S7).

193 The beginning of Phase II is defined by the first appearances of faecal biomarkers such as 5 β -
194 stigmastanol at ca. 700 ± 60 CE in the Lake Peixinho sedimentary record ($50 \text{ ng cm}^{-2} \text{y}^{-1}$ Pico
195 Island, Central Island Group), and at 850 ± 60 CE in Lake Caldeirão ($69 \text{ ng cm}^{-2} \text{y}^{-1}$ Corvo Island,
196 Western Island Group). These biomarkers provide the most direct evidence, likely introduced
197 livestock (e.g. cattle, sheep, goats, and pigs), and provide the most direct evidence to date for the
198 first human activities on the islands (Fig. 2). Furthermore, given the distances between these two
199 islands (~ 260 km), the near synchronous appearance of the faecal markers in these two lake
200 systems suggests that, within chronological uncertainties, the arrival of early human settlers was
201 nearly synchronous across the archipelago.

202 The sudden and synchronous appearance of faecal biomarkers in the records on the distant Pico
203 and Corvo Islands contrasts with the lack of faecal biomarkers at Flores Island until 1300 CE,
204 although this island is only ca. 30 km south of (and visible from) Corvo Island. One possible
205 explanation could be hydrological differences. In contrast to Flores Island, neither Pico nor Corvo
206 Island have a well-developed surface hydrological system with permanent streams that transport
207 freshwater from the highlands to the shore. Consequently, highland lakes from Pico and Corvo
208 Island may have been the primary source of freshwater when the first settlements were
209 established, while they were probably less important when Flores Island was first occupied. In
210 addition, the patterns of human land use for volcanic islands usually follow an altitudinal
211 stratification resulting from a combination of a generally uneven orography and variation of bio-
212 climatic conditions with altitude (28, 29). This appears to be the case for the Azores Archipelago
213 islands in historical records (30) and could have also played a role during the early colonization of
214 these islands, with the first settlers only occupying and/or exploiting the islands' highlands when
215 strictly necessary.

216 Livestock faecal sterols are continuously present from 950.₋₆₀⁺⁵⁰ CE onwards in Lake Peixinho,
217 although they show a more punctuated presence in Lake Caldeirão (Fig. 2). The simultaneous
218 increase of pyrolytic PAHs and macrocharcoal suggest that slash-and-burn techniques was used
219 to create suitable pastures for livestock close to the lake shores. This interpretation is reinforced
220 by the influx of arboreal plant macrofossils in Lake Caldeirão (*SI Appendix*, Fig. S1) and pollen in
221 Lake Peixinho (*SI Appendix*, Fig. S3), which show a sudden decline in juniper forests and an
222 expansion of grasses (Poaceae) at that time. Proxy-based indicators in lake sediments suggest
223 that the initial appearance of humans/livestock on the islands (Phase II; Fig. 2) was quickly
224 followed by large-scale landscape modifications and the introduction of large ruminants,
225 presumably associated with the establishment of permanent settlements.

226 The introduction of livestock and the practice of slash-and-burn agriculture had significant
227 ecological impacts on aquatic systems in the Azores Archipelago, as has been observed for other
228 island systems (31). The rise in the dominance of mesotrophic tycho planktonic diatoms in Lake
229 Peixinho, together with the presence of profundal and low oxygen tolerance associated
230 chironomid taxa, and the decrease from 2.8 ± 0.4 ‰ to 1.9 ± 0.4 ‰ in $\delta^{15}\text{N}$ values, indicates a
231 rise in lake trophic state (see *SI Appendix*, Fig. S3). However, impacts on lake ecology appear to
232 be site dependent, with similar paleolimnological proxy indicators remaining relatively unchanged
233 in Lake Caldeirão at this time, perhaps because local settlements were either small or temporary.

234 The first appearance of coprostanol occurs at the beginning of Phase III at ca. 1070 CE in Lake
235 Peixinho ($8.4 \text{ ng cm}^{-2} \text{ y}^{-1}$ Pico Island), and at 1280 CE in Lake Azul ($6.5 \text{ ng cm}^{-2} \text{ y}^{-1}$ São Miguel
236 Island) (Fig. 2). These records provide unequivocal evidence of substantial human occupation
237 and are associated with unprecedented changes in the catchments and the lakes over the last
238 1500 years. Lake sediments of Pico, Corvo, Flores, and São Miguel islands all show a sharp drop
239 in arboreal pollen and a drastic increase of *Juniperus* leaf influx, in conjunction with an increase in
240 5β -stigmastanol, coprophilous fungi, pyrolytic PAH, and charcoal particles (Fig. 2). Taken
241 together, this suggests that as human population pressure increased, deforestation intensified to
242 clear space for agriculture and livestock. The first appearance of *Secale cereale* pollen grains ca.
243 1150 CE in Pico, ca. 1300 CE in São Miguel, and ca. 1550 CE in Corvo, as well as *Plantago* spp.
244 in Pico (ca. 1170 CE) and Corvo (ca. 1390 CE), corroborates this interpretation (*SI Appendix*, Fig.
245 S1-S5). The intensification of human activities also resulted in an ecological regime shifts in
246 Lakes Caldeirão, Funda, and Peixinho as evidenced by accelerated sedimentation rates, higher

247 concentrations of terrigenous elements (Ti, Fe, Mn), and an increase in the relative abundance of
248 aerophilic diatoms of allochthonous origin (see *SI Appendix*, Fig. S1-S5). Increased erosion and
249 runoff from the catchment modified the supply of dissolved organic matter to the lakes, increased
250 nutrient availability, altered aquatic communities, and drastically increased lake productivity. A
251 decrease in sediment TOC/TN ratios at this time indicates a transition towards more lacustrine-
252 dominated organic matter in association with higher nutrient levels (*SI Appendix*, Fig. S7).

253 The CESM Last Millennium simulations for this time interval suggest that the intensification of
254 anthropogenic pressures on local ecosystems occurred during a period of enhanced aridity partly
255 due to the predominance of positive phases of the North Atlantic Oscillation and East Atlantic
256 pattern (NAO⁺/EA⁺) (*SI Appendix*). Combined positive NAO and positive EA phases (*SI Appendix*,
257 Fig. S10) resulted in lower-than-average temperatures over Iceland, Greenland, and North Africa
258 and higher-than-average temperatures in the British Isles, Scandinavia, and eastern North
259 Atlantic (including the Azores Archipelago). Warmer and drier conditions at this time in the Azores
260 might have forced the inhabitants to exploit less accessible lakes located in the central and
261 highland areas of islands, such as on Flores Island, to aid in their survival, leading to an increase
262 in disturbance indicators in their sediment records.

263 Phase IV began with the historically documented arrival of the Portuguese to the Archipelago
264 between 1430 and 1450 CE and, consolidated the profound ecological transformation of
265 terrestrial and lacustrine ecosystems initiated during the previous phase (Fig. 2 and *SI Appendix*,
266 Fig. S1-S5). The steady decline of native arboreal pollen favored the appearance of grass
267 meadows mostly dominated by Poaceae. The continuous presence of coprophilous dung fungal
268 spores of *Sporormiella*-type in the sedimentary records confirms the intensification of human
269 activities including forest burning, cereal cultivation, and animal husbandry, as recorded in
270 Portuguese historical documents (2, 15). In contrast to previous intervals, this further
271 intensification of human activities often resulted in irreversible changes to lake trophic states.
272 Increased catchment erosion resulted in enhanced delivery of nutrients to most lakes, leading to
273 increased eutrophication, as indicated by a larger abundance of eutrophic diatom taxa, and the
274 development of a more permanent anoxic hypolimnion as evidenced by a reduction in chironomid
275 abundances (see *SI Appendix*, Fig. S1-S5). Successive introductions of fish in the fishless lakes
276 of the Azores after 1790 CE triggered a set of top-down (predation on zooplankton and
277 chironomids) and bottom-up (sediment-resuspension) controls, promoting a further shift towards
278 eutrophic conditions (32, 33).

279 The arrival of the Portuguese to the Azores occurred during the Little Ice Age (LIA; 1300-1850
280 CE, (34)). Simulations with CESM indicate that this interval was marked by a more dominant
281 NAO⁻/EA⁺ atmospheric winter configuration, resulting in a tendency towards more humid and
282 colder-than-average climate conditions on the Azores Archipelago (Figure 3 and S11). The shift
283 to wetter conditions is evident in the aquatic diatom records, particularly in the deeper lake
284 systems (i.e., Lakes Funda and, Azul). Despite the evidence for milder climate conditions at this
285 time, disturbance indicators still increase, demonstrating the severity of the impacts of
286 Portuguese settlement. However, the shift in climate conditions likely also enhanced surficial
287 runoff, exacerbating the anthropogenic effects on the freshwater ecosystems.

288 **Who first colonized the Azores?**

289 Our reconstructions offer unambiguous evidence for the pre-Portuguese settlement of the Azores
290 Archipelago and suggests that people first occupied the islands as early as the Early Middle Ages
291 (EMA; 500 – 900 CE), This finding builds upon other studies suggesting that the Portuguese may

292 not have been the first inhabitants of the islands. Previous work on lake sediments from Lake
293 Azul, on São Miguel Island, using pollen, charcoal and dung fungi as proxy-based indicators,
294 demonstrated that rye pollen together with spores from coprophilous fungi (*Sordaria*,
295 *Sporormiella*, *Cercophora*, *Podospora*) were continuously present after 1287 CE and were
296 interpreted as evidence of early cereal cultivation and livestock farming, respectively (25). Our
297 current study extends the timing of the earliest occupation by human back by an additional 500
298 years. Other recent data supports our new evidence for initial occupation in the Early Middle
299 Ages. For example, a recent radiocarbon date 903-1036 CE (1033 ± 28 yr BP uncalibrated) on
300 house-mouse (*Mus musculus*) bones collected at a fossil site on Madeira Island (35) and
301 colonization dates of 910-1185 CE for this species established by molecular dating methods
302 using mtDNA D-loop sequences (36) suggest that explorers had accidentally introduced this alien
303 species on several Macaronesian islands by this time (Azores, Madeira, and the Canary Islands).
304 Although controversial, radiocarbon dating of organic matter embedded in silica cement that
305 partially filled a putative human-made trachytic rock bowl from Terceira Island yielded an age of
306 1020 - 1160 CE (950 ± 30 cal. yr BP, $2\text{-}\sigma$) (37). These studies are consistent with the first
307 appearance of faecal biomarkers in our records (Fig. 4).

308 Genetic characterization of modern Macaronesian *Mus musculus* populations present in the
309 Azores shows that this species followed a complex colonization history from multiple
310 geographical origins (38), with two of the mitochondrial D-loop sequences indicating an origin in
311 northern Europe (Denmark, Norway, Iceland, Ireland, Sweden, Finland, and the Faroe Islands)
312 (39). The observation that northern European mice contribute significantly to the Azorean mouse
313 gene pool suggests that they were amongst the earliest populations introduced to the island.
314 This strongly suggests that they arrived with the earliest settlers, from northern Europe, in the
315 early Middle Ages. An early discovery of the Macaronesian islands by the Norse from northern
316 Europe also provides a plausible explanation for the presence of the archipelago on maps before
317 the official Portuguese discovery. In fact, Corvo island appears as *Corvis Marinis* (Marine Raven
318 Island) in the Medici Atlas (1370 CE), suggesting that Northern people discovered it since these
319 northern explorers usually used ravens to help them locate landfalls when far out at sea (40).

320 To better understand the climatic and oceanic conditions under which this early arrival may have
321 occurred, we examined climate model simulations for the 850-1850 CE period using the CESM-
322 CAM5_CN from the LME (21). According to this climate model simulation, the end of the EMA
323 period was associated with a predominance of NAO⁻/EA⁻ phases (41, 42), with warmer and drier-
324 than-average decadal climate conditions (Fig. 3 and *SI Appendix*, Fig. S8). This prevailing
325 NAO/EA combination resulted in a Mean Sea Level Pressure (MSLP) dipole with severely
326 weakened westerly winds over all the North Atlantic (25 °- 65 °N) and an enhanced northerly wind
327 component following the N - S western European margin, from Scandinavia to the Iberian
328 Peninsula (Fig. 3 and *SI Appendix*, Fig. S11). The weakening of the westerlies associated with
329 anomalous NE winds would have facilitated the arrival of Norse explorers to the Archipelago,
330 while hindering more meridional explorers from reaching these islands. At that time, the Norse
331 started to colonize North Atlantic islands, with settlements in the Faroe Islands (ca. 800 CE),
332 Iceland (ca. 870 CE), Greenland (ca. 1000 CE), and Newfoundland (ca. 1000 CE) (43, 44).
333 Therefore, they had the knowledge and navigational skills required to sail in open ocean waters
334 and are the most likely candidates to have reached the Azores Archipelago during this period.
335 The lack of historical records prevents us from concluding whether their arrival on the Azores
336 Archipelago was intentional (very unlikely, as the first known maps detailing the approximate

337 location of the islands were drawn 500 years later) or accidental (more probable as storms and
338 anomalous NE winds might have sporadically pushed ships out of their common sailing routes).

339 The EMA's atmospheric configuration is different from what was typical of the time period when
340 the Portuguese officially colonized the Azores. Between 1430 and 1450 CE, the multi-decadal
341 dominance of the NAO/EA⁺ phases led to weakened westerlies with prevailing SE winds that
342 favored navigation between southern Europe and the Azores Archipelago, while pushing northern
343 explorers towards the American continent (Fig. 3). This particular NAO/EA combination at the
344 onset of the LIA triggered an MSLP dipole with higher-than-usual MSLP values over Iceland and
345 lower-than-usual MSLP values over the central Atlantic. These MSLP anomalies gave rise to a
346 southern migration of an enhanced westerlies belt (< 30 °N), resulting in strongly weakened
347 westerlies between 35° and 60° N (see SI appendix). Therefore, the two main colonization pulses
348 were facilitated by weakened westerlies due to a NAO⁻ phase predominance, whereas the
349 (negative or positive) EA pattern phase likely played a key role in determining who (Norse or
350 Portuguese) and when (9th or 15th centuries, respectively) the first explorers reached and settled
351 the Azores Archipelago.

352 The results of this study suggest that early settlers from northern Europe not only reached the
353 Azores several hundreds of years before the Portuguese, but that their settlements were
354 extensive enough to be evident in faecal biomarker records in sites throughout the archipelago.
355 Furthermore, these early settlements led to profound environmental and ecological disturbance
356 (8). These findings are in conflict with the reports of early Portuguese sailors, who described the
357 Azores as heavily forested and pristine. Given the much more extensive environmental
358 degradation which accompanied Portuguese arrival, it may be that comparatively unaltered
359 conditions of the islands appeared undisturbed to the first Portuguese settlers. This highlights the
360 challenge in relying on the historical record to identify relative states of ecosystems or landscape
361 disturbance (8). Another question raised by the data is the persistence of faecal biomarkers in the
362 lake records up to the time of Portuguese arrival, when there are no reports of human occupation
363 or introduced ruminants (2, 3). Such long-lasting occupations should be evident in the
364 archaeological record. More work on this possibility is needed in the future.

365 **Materials and Methods**

366

367 Coring campaigns were conducted in September 2011 (Lake Azul), July 2015 (Lake Peixinho),
368 June 2017 (Lakes Funda and Caldeirão), and August 2018 (Lake Ginjal) to retrieve the complete
369 sedimentary infill using a UWITEC piston corer installed on a UWITEC floating platform. Cores
370 were sealed entirely in the field and transported to Geo3BCN-CSIC (Barcelona, Spain). They
371 were split longitudinally, imaged with a high-resolution CCD camera, and their elemental chemical
372 composition determined every 2 mm using an AVAATECH XRF continuous core scanner at the
373 University of Barcelona. Cores were subsampled regularly to assess the content of pollen and
374 other non-palynological remains, micro, and macrocharcoal, chironomids, diatoms, bulk organic
375 matter composition (TOC and TN), isotope signatures ($\delta^{13}\text{C}$ and $\delta^{15}\text{N}$), mineralogical
376 composition, and sterol and stanol analyses. See the SI Appendix for further details of the
377 methodologies and sampling intervals employed to characterize these proxies.

378 To understand the climate conditions under which changes in occupation and disturbance
379 occurred, we use results from the Last Millennium Ensemble (LME) using CESM-CAM5_CN. We
380 selected this model as it provides simulations using transient forcing mechanisms, and according
381 to its spatio-temporal resolution (2° horizontal and monthly) and the available climate variables

382 (mean sea level pressure, horizontal wind at the 925 hPa level, 2 m air temperature, and
383 precipitation). We acknowledge that these simulations start only at 850 CE, but we are unaware
384 of any similar simulations extending back to the previous century when our data suggest that first
385 occupation of the Azores occurred (i.e., 700-850 CE). Thus, we use the earliest available period
386 of simulation (850-900 CE) to characterize the conditions under which the initial colonization
387 occurred. Given the small changes in forcing applied in the transient simulations during these two
388 centuries (700-900 CE), we are confident that this should be a relatively close approximation to
389 the interval of interest. Further details related to the CESM simulations are detailed in the
390 supplementary material.

391 The chronological framework for the records was built using four ^{210}Pb and three ^{137}Cs profiles,
392 and 40 AMS ^{14}C dates. The statistical analyses of the proxy-based indicators and the age-depth
393 model for every record, integrating ^{210}Pb and ^{137}Cs profiles and the radiocarbon dating on plant
394 macrofossil remains, and pollen concentrates, were carried out using the version 2.3.9 of the R
395 Clam package (45, 46), (47). This package automatically calibrated all radiocarbon dates at 2- σ
396 using the IntCal20 calibration curve (48).

397 **Acknowledgments**

398 This research is funded by Fundação para a Ciência e Tecnologia (DL57/2016/
399 ICETA/EEC2018/25) and DISCOVERAZORES (PTDC/CTA-AMB/28511/2017), and through the
400 funded by the Spanish Ministry of Economy and Competitiveness projects PaleoNAO (CGL2010-
401 15767), RapidNAO (CGL2013-40608-R), and PaleoModes (CGL2016-75281-C2) and by the
402 Luso-American Foundation. This work is contributing to the ICTA's "Unit of Excellence" Maria de
403 Maetzu (CEX2019-000940-M). The IAEA is grateful for the support provided to its Environment
404 Laboratories by the Government of the Principality of Monaco.

405

406 **References**

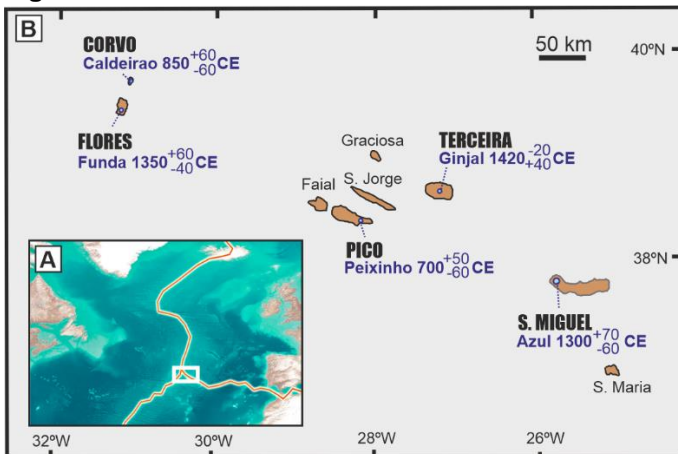
- 407 1. J. Adam, J. Ronnby, "The Consequences of New Warships – From Medieval to Modern
408 and our Dialectical Relationship with Things" in *On War on Board - Archaeological and
409 Historical Perspectives on Early Modern Maritime Violence and Warfare*, J. Ronnby, Ed.
410 (Södertörns högskola, 2019), pp. 163–198.
- 411 2. G. Frutuoso, *Livro Quarto das Saudades da Terra* (Instituto Cultural de Ponta Delgada,
412 1981).
- 413 3. G. Frutuoso, *Livro Sexto das Saudades da Terra*, Instituto (1978).
- 414 4. G. Frutuoso, *Livro Terceiro das Saudades da Terra*, Instituto (1983).
- 415 5. A. T. Matos, "Povoamento e colonização dos Açores" in *Portugal No Mundo*, L. de
416 Albuquerque, Ed. (Alfa, 1989), pp. 176–188.
- 417 6. A. de F. de Meneses, Os Açores e os Impérios - séculos XV a XX. *Arquipélago - História*
418 **XIII**, 205–218 (2009).
- 419 7. E. Dias, *et al.*, "Espécies florestais das ilhas - Açores" in *Árvores e Florestas de Portugal*,
420 J. S. Silva, Ed. (Público, Comunicação Social, SA/ Fundação Luso-Americana/ Liga para
421 a Protecção da Natureza., 2007), pp. 199–254.
- 422 8. S. Nogué, *et al.*, The human dimension of biodiversity changes on islands. *Science* **372**,
423 488 LP – 491 (2021).

- 424 9. R. M. D'Anjou, R. S. Bradley, N. L. Balascio, D. B. Finkelstein, Climate impacts on human
425 settlement and agricultural activities in northern Norway revealed through sediment
426 biogeochemistry. *Proc. Natl. Acad. Sci.* **109**, 20332–20337 (2012).
- 427 10. C. G. Daughton, Real-time estimation of small-area populations with human biomarkers in
428 sewage. *Sci. Total Environ.* **414**, 6–21 (2012).
- 429 11. R. Leeming, A. Ball, N. Ashbolt, P. Nichols, Using faecal sterols from humans and animals
430 to distinguish faecal pollution in receiving waters. *Water Res.* **30**, 2893–2900 (1996).
- 431 12. I. D. Bull, M. J. Lockheart, M. M. Elhmmali, D. J. Roberts, R. P. Evershed, The origin of
432 faeces by means of biomarker detection. *Environ. Int.* **27**, 647–654 (2002).
- 433 13. O. K. Davis, Spores of the Dung Fungus *Sporormiella*: Increased Abundance in Historic
434 Sediments and Before Pleistocene Megafaunal Extinction. *Quat. Res.* **28**, 290–294
435 (1987).
- 436 14. A. G. Baker, S. A. Bhagwat, K. J. Willis, Do dung fungal spores make a good proxy for
437 past distribution of large herbivores? *Quat. Sci. Rev.* **62**, 21–31 (2013).
- 438 15. J. M. Moreira, *Alguns aspectos de intervenção humana na evolução da paisagem da ilha*
439 *de S. Miguel (Açores)* (Serviço Nacional de Parques, Reservas e Conservação da
440 Natureza, 1987).
- 441 16. J. P. Smol, H. J. B. Birks, W. M. Last, R. S. Bradley, K. Alverson, *Tracking Environmental*
442 *Change Using Lake Sediments Terrestrial, Algal, and Siliceous Indicators* (Kluwer
443 Academic Publishers, 2005).
- 444 17. E. H. Denis, *et al.*, Polycyclic aromatic hydrocarbons (PAHs) in lake sediments record
445 historic fire events: Validation using HPLC-fluorescence detection. *Org. Geochem.* **45**, 7–
446 17 (2012).
- 447 18. W. M. Last, J. P. Smol, *Tracking Environmental Change Using Lake Sediments - Physical*
448 *and Geochemical Methods* (Kluwer Academic Publishers, 2002).
- 449 19. P. M. Raposeiro, A. Sáez, S. Giral, A. C. Costa, V. Gonçalves, Causes of spatial
450 distribution of subfossil diatom and chironomid assemblages in surface sediments of a
451 remote deep island lake. *Hydrobiologia* **815**, 141–163 (2018).
- 452 20. D. Vázquez-Loureiro, *et al.*, Diatom-inferred ecological responses of an oceanic lake
453 system to volcanism and anthropogenic perturbations since 1290 CE. *Palaeogeogr.*
454 *Palaeoclimatol. Palaeoecol.* **534**, 109285 (2019).
- 455 21. B. L. Otto-Bliesner, *et al.*, Climate variability and change since 850 C.E.: An ensemble
456 approach with the Community Earth System Model (CESM). *Bull. Am. Meteorol. Soc.*,
457 735–754 (2016).
- 458 22. S. E. Connor, *et al.*, The ecological impact of oceanic island colonization - a
459 palaeoecological perspective from the Azores. *J. Biogeogr.* **39**, 1007–1023 (2012).
- 460 23. S. Björck, *et al.*, A Holocene lacustrine record in the central North Atlantic: proxies for
461 volcanic activity, short-term NAO mode variability, and long-term precipitation changes.
462 *Quat. Sci. Rev.* **25**, 9–32 (2006).

- 463 24. M. Masseti, Mammals of the Macaronesian islands (the Azores, Madeira, the Canary and
464 Cape Verde islands): redefinition of the ecological equilibrium. *74*, 3–34 (2010).
- 465 25. V. Rull, *et al.*, Vegetation and landscape dynamics under natural and anthropogenic
466 forcing on the Azores Islands: A 700-year pollen record from the São Miguel Island. *Quat.*
467 *Sci. Rev.* **159**, 155–168 (2017).
- 468 26. S. E. Connor, *et al.*, The ecological impact of oceanic island colonization—a
469 palaeoecological perspective from the Azores. *J. Biogeogr.* **39**, 1007–1023 (2012).
- 470 27. J. F. N. van Leeuwen, *et al.*, Native or introduced? Fossil pollen and spores may say. An
471 example from the Azores Island. *Neobiota* **6**, 27–34 (2005).
- 472 28. W. D. Gosling, *et al.*, Human occupation and ecosystem change on Upolu (Samoa) during
473 the Holocene. *J. Biogeogr.* **47**, 600–614 (2020).
- 474 29. D. Kennett, A. Anderson, M. Prebble, E. Conte, J. Southon, Prehistoric human impacts on
475 Rapa, French Polynesia. *Antiquity* **80**, 340–354 (2006).
- 476 30. R. Fernandes, P. Pinho, The distinctive nature of spatial development on small islands.
477 *Prog. Plann.* **112**, 1–18 (2017).
- 478 31. D. B. McWethy, *et al.*, Rapid landscape transformation in South Island, New Zealand,
479 following initial Polynesian settlement. *Proc. Natl. Acad. Sci.* **107**, 21343 LP – 21348
480 (2010).
- 481 32. P. M. Raposeiro, *et al.*, Impact of the historical introduction of exotic fishes on the
482 chironomid community of Lake Azul (Azores Islands). *Palaeogeogr. Palaeoclimatol.*
483 *Palaeoecol.* **466**, 77–88 (2017).
- 484 33. T. Skov, *et al.*, Using invertebrate remains and pigments in the sediment to infer changes
485 in trophic structure after fish introduction in Lake Fogo: a crater lake in the Azores.
486 *Hydrobiologia* **654**, 13–25 (2010).
- 487 34. M. Oliva, *et al.*, The Little Ice Age in Iberian mountains. *Earth-Science Rev.* **177**, 175–208
488 (2018).
- 489 35. J. C. Rando, H. Pieper, J. A. Alcover, Radiocarbon evidence for the presence of mice on
490 Madeira Island (North Atlantic) one millennium ago. *Proc. R. Soc. B* **281**, 20133126
491 (2014).
- 492 36. D. W. Förster, *et al.*, Molecular insights into the colonization and chromosomal
493 diversification of Madeiran house mice. *Mol. Ecol.* **18**, 4477–4494 (2009).
- 494 37. A. F. Rodrigues, N. O. Martins, N. Ribeiro, A. Joaquineto, Early Atlantic navigation: Pre-
495 Portuguese presence in the Azores Islands. *Archaeol. Discov.* **03**, 104–113 (2015).
- 496 38. S. I. Gabriel, M. L. Mathias, J. B. Searle, Of mice and the “Age of Discovery”: The complex
497 history of colonization of the Azorean archipelago by the house mouse (*Mus musculus*) as
498 revealed by mitochondrial DNA variation. *J. Evol. Biol.* **28**, 130–145 (2015).
- 499 39. C. Santos, *et al.*, Genetic structure and origin of peopling in the Azores Islands (Portugal):
500 the view from mtDNA. *Ann. Hum. Genet.* **67**, 433–456 (2003).

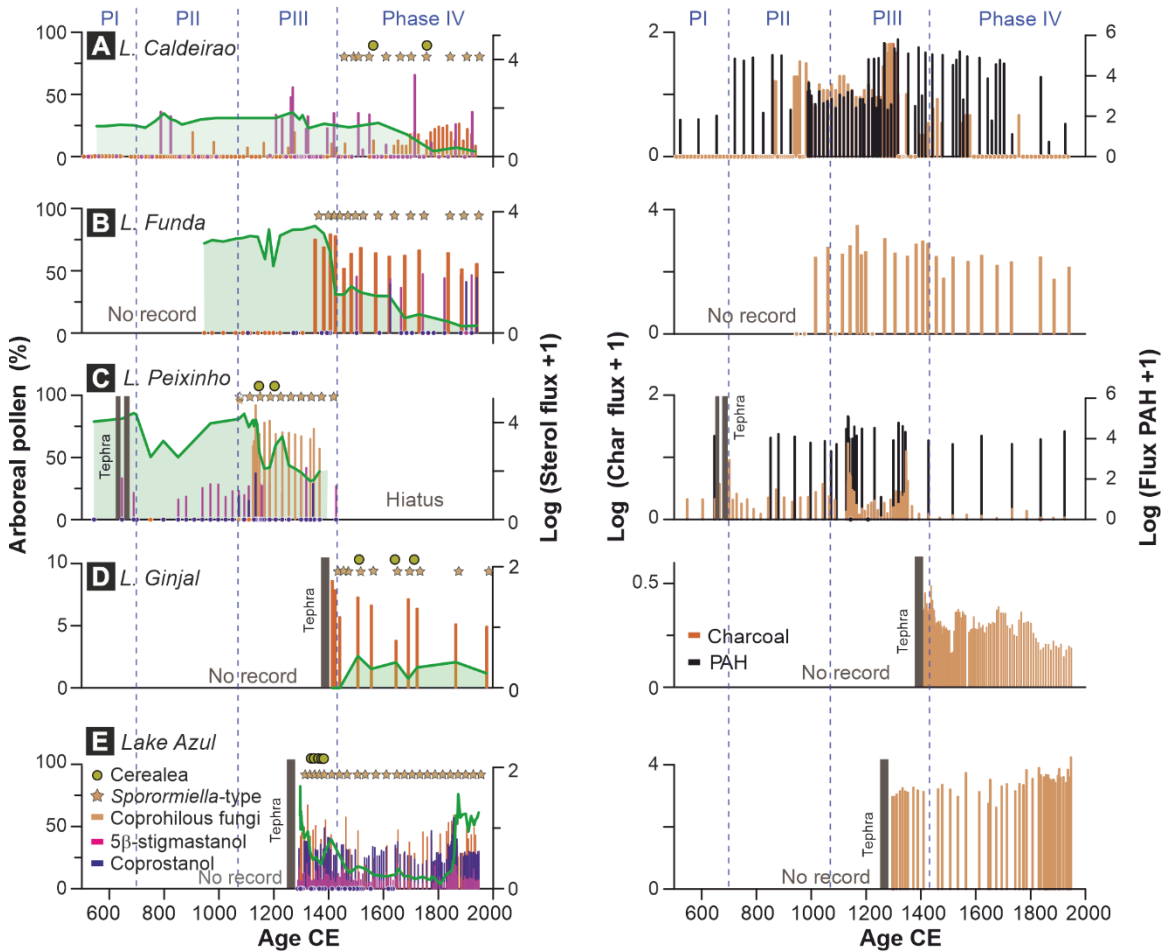
- 501 40. J. E. Kelley Jr, Non-Mediterranean influences that shaped the Atlantic in the early Portolan
502 charts, *Imago Mundi. Int. J. Hist. Cartogr.* **31**, 18–35 (1979).
- 503 41. J. Mellado-Cano, D. Barriopedro, R. García-Herrera, R. M. Trigo, A. Hernández,
504 Examining the North Atlantic Oscillation, East Atlantic pattern, and Jet variability since
505 1865. *J. Clim.* **32**, 6285–6298 (2019).
- 506 42. P. Ortega, *et al.*, A model-tested North Atlantic Oscillation reconstruction for the past
507 millennium. *Nature* **523**, 71–74 (2015).
- 508 43. A. J. Dugmore, C. Keller, T. H. McGovern, Norse Greenland settlement: reflections on
509 climate change, trade, and the contrasting fates of human settlements in the North Atlantic
510 islands. *Arctic Anthropol.* **44**, 12–36 (2007).
- 511 44. S. Brink, N. Price, *The Viking World* (Routledge Taylor and Francis Group, 2018).
- 512 45. M. Blaauw, Methods and code for “classical” age-modelling of radiocarbon sequences.
513 *Quat. Geochronol.* **5**, 512–518 (2010).
- 514 46. M. Blaauw, clam: Classical Age-Depth Modelling of Cores from Deposits (2020).
- 515 47. R Core Team, R: A Language and Environment for Statistical Computing (2020).
- 516 48. P. J. Reimer, *et al.*, The IntCal13 Northern Hemisphere radiocarbon age calibration curve
517 (0-55 cal kBP. *Radiocarbon* **62**, 725–757 (2020).
- 518
- 519

520 **Figures**



521 **Figure 1.** (A) Inset: Location of the Azores Archipelago in the North Atlantic. Red lines – Triple
522 junction between North American, the Eurasian and the Nubian plates. (B) Large figure:
523 Distribution of the islands in the Western Group (Corvo and Flores Islands), Central Group (São
524 Jorge, Faial, Graciosa, Terceira, and Pico Islands), and Eastern Group (São Miguel and Santa
525 Maria Islands). Islands and lakes from which sediment records have been studied.
526 The dates for each lake correspond to the first appearance of unequivocal evidence of human
527 activities (see text for further details).
528
529

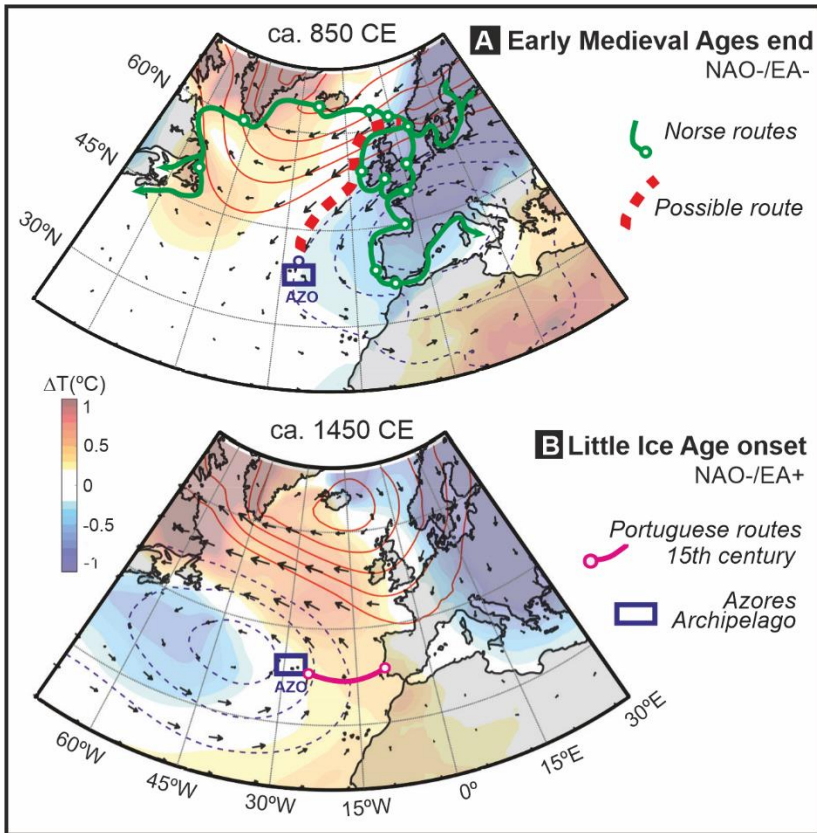
530



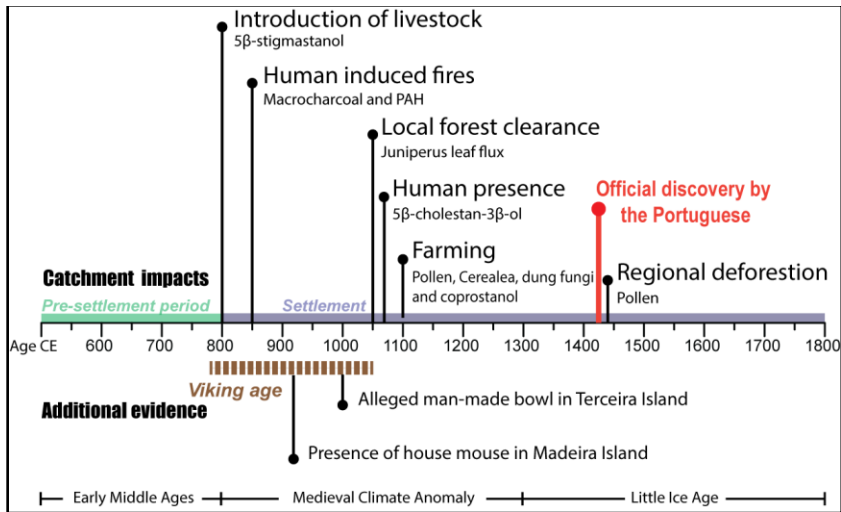
531

Figure 2. Left – Faecal sterol biomarkers coprostanol (Blue bar) (5β -cholestan- 3β -ol) and 5β -stigmastanol flux (Magenta bar) ($\text{ng cm}^{-2} \text{y}^{-1}$), Coprophilous fungi flux (Orange bar) ($\text{spores cm}^{-2} \text{y}^{-1}$), Arboreal pollen (%; Green line and silhouette), presence of Cerealea pollen (Yellow dot) and Sporormiella-type fungi (Star). Right - Total pyrolytic PAHs flux (Black bar) ($\text{ng cm}^{-2} \text{y}^{-1}$) and charcoal flux (Orange bar) ($\text{particles cm}^{-2} \text{y}^{-1}$). Western Group A) Lake Caldeirão (Corvo Island); B) Lake Funda (Flores Island); Central Group C) Lake Peixinho (Pico Island); D) Lake Ginjal (Terceira Island) and Eastern Group E) Lake Azul (São Miguel Island). Phases: I – Absence of faecal biomarkers; II – First appearance of faecal biomarkers; III – First appearance of coprostanol (5β -cholestan- 3β -ol); IV – Official Portuguese arrival to Azores Archipelago. Grey bars, represent tephra layers.

532



533
 534 **Figure 3.** North Atlantic average anomalies for Mean Sea Level Pressure (MSLP; blue/red lines),
 535 2 m temperature (shading), and 925 hPa horizontal wind (vectors) during the 850 – 1500 CE
 536 period. **A)** Average anomalies for MSLP (blue/red lines), 2 m temperature (shading), and 925 hPa
 537 horizontal wind (vectors) during NAO-/EA⁻ prevailing conditions. Greenline - Norse maritime
 538 routes during the 9th-11th century. Blue rectangle – location of the Azores Archipelago (AZO).
 539 Dotted orange - a possible route of Norse reaching the Azores Archipelago. **B)** Average
 540 anomalies for MSLP (blue/red lines), 2 m temperature (shading), and 925 hPa horizontal wind
 541 (vectors) during NAO-/EA⁺ prevailing conditions. Magenta line - Portuguese maritime routes
 542 during 15th century. Blue rectangle – Azores Archipelago location.
 543



544
545
546
547
548

Figure 4. Summary of evidence for earlier human activities and the timing of the Portuguese arrival in the Azorean Archipelago between 500 – 1800 CE.

Supplementary Information for

Climate change facilitated the early colonization of the Azores Archipelago during Medieval times.

Pedro M. Raposeiro^{a,b*}, Armand Hernández^c, Sergi Pla-Rabes^d, Vítor Gonçalves^{a,b}, Roberto Bao^e, Alberto Sáez^f, Timothy Shanahan^g, Mario Benavente^c, Erik J. de Boer^f, Nora Richter^{h,i}, Verónica Gordonⁱ, Helena Marques^{a,b}, Pedro M. Sousa^{j,k}, Martín Souto^{a,b}, Miguel G. Matias^{l,m}, Nicole Aguiar^b, Cátia Pereira^{l,m}, Catarina Ritter^{a,b}, María Jesús Rubio^c, Marina Salcedo^b, David Vázquez-Loureiro^e, Olga Margalef^{d,f}, Linda A. Amaral-Zettler^{h,i,n}, Ana Cristina Costa^{a,b}, Yongsong Huang^l, Jacqueline FN van Leeuwen^o, Pere Masqué^{p,q,r}, Ricardo Prego^s, Ana Carolina Ruiz-Fernández^t, Joan-Albert Sánchez-Cabeza^l, Ricardo Trigo^k, and Santiago Giralt^c

^a CIBIO, Centro de Investigação em Biodiversidade e Recursos Genéticos, InBIO Laboratório Associado, Pólo dos Açores, Rua da Mãe de Deus, 9500-321 Ponta Delgada, Portugal

^b Faculdade de Ciências e Tecnologia, Universidade dos Açores, Rua da Mãe de Deus, 9500-321 Ponta Delgada, Portugal

^c Geosciences Barcelona (Geo3BCN-CSIC), Lluís Solé i Sabarís s/n, 08028 Barcelona, Spain

^d CREA, Campus de Bellaterra (UAB), Edifici C, 08193, Cerdanyola del Valles, Spain

^e Centro de Investigacións Científicas Avanzadas (CICA), Facultade de Ciencias, Campus da Zapateira s/n, Universidade da Coruña, 15071 A Coruña, Spain

^f Department de Dinàmica de la Terra i de l'Oceà, Facultat de Ciències de la Terra, Universitat de Barcelona, Martí i Franquès s/n, 08028 Barcelona, Spain

^g Department of Geosciences, University of Texas at Austin, Austin, TX 78712, USA

^h NIOZ Royal Netherlands Institute for Sea Research, P.O. Box 59, 1790 AB Den Burg, The Netherlands

ⁱ Department of Earth, Environmental and Planetary Sciences, Brown University, Providence, RI 02912, USA

^j Instituto Português do Mar e da Atmosfera (IPMA), 1749-077 Lisboa, Portugal

^k Instituto Dom Luiz (IDL), Faculdade de Ciências, Universidade de Lisboa, 1749-016 Lisbon, Portugal

^l Departamento de Biogeografía y Cambio Global, Museo Nacional de Ciencias Naturales, CSIC, Madrid, Spain

^m Biodiversity Research Chair - MED – Mediterranean Institute for Agriculture, Environment and Development. Universidade de Évora, Rua Dr. Joaquim Henrique da Fonseca. Casa do Cordovil, N^o7, 2^o Andar. 7000-890, Évora, Portugal

ⁿ Department of Freshwater and Marine Ecology, Institute for Biodiversity and Ecosystem Dynamics, University of Amsterdam, The Netherlands

^o Institute of Plant Sciences and Oeschger Center for Climate Change Research, University of Bern, Switzerland

^p International Atomic Energy Agency, 4a Quai Antoine 1er, 98000 Principality of Monaco, Monaco

^q Institute of Environmental Science and Technology (ICTA) and Physics Department, Universitat Autònoma de Barcelona, Bellaterra, 08193, Spain

^r School of Natural Sciences, Centre for Marine Ecosystems Research, Edith Cowan University, Joondalup, WA 6027, Australia

^s Department of Oceanography, Marine Research Institute (CSIC), 36208 Vigo, Spain

^t Universidad Nacional Autónoma de México, Instituto de Ciencias del Mar y Limnología, Unidad Académica Mazatlán, Calz. J. Montes Camarena s/n, 82040 Mazatlán, Mexico

*Pedro M. Raposeiro.

Email: pedro.mv.raposeiro@uac.pt

This PDF file includes:

Supplementary text

Figures S1 to S11 (not allowed for Brief Reports)

Tables S1 to S2 (not allowed for Brief Reports)

SI References

Origin, climatology and modern ecology

The Azores Archipelago (Portugal; northeast Atlantic Ocean; 36°55–39°43N, 24°46–31°16W) consists of nine islands and several islets that are divided into three groups: the western group (Flores and Corvo), the central group (Terceira, Faial, São Jorge, Pico, and Graciosa), and the eastern group (São Miguel, Santa Maria). The archipelago spans 615 km and is located 1300 km west of Portugal and 1900 km east of North America. The ages of all islands range from 5.5 million years for Santa Maria (1) to 0.27 million years for Pico (2).

Climate

The climate of the Azores Archipelago is considered marine temperate and characterized by mild temperatures with minor annual variations. The rainfall regime displays a solid seasonal cycle and large interannual variability, high relative air humidity, and frequent strong winds (3, 4). The climatic conditions are determined by the strength and position of the Azores Current and the a semi-permanent high-pressure system known as the Azores Anticyclone (5). Most of its winter climate variability is determined by the NAO, which has its southern end on the archipelago (4, 6, 7). However, when the NAO influence becomes weaker, the effects of other large-scale climate modes of variability appear to increase, highlighting the non-stationary influence of the NAO on the Azorean climate (4, 8).

Natural vegetation

Before the human arrival, the landscape was dominated by dense laurisilva forests dominated by short-stature trees of *Juniperus brevifolia* and *Morella faya* (9–12). Throughout the centuries of human settlement, the Azores have been drastically deforested to create space for agricultural fields, supply energy for people (charcoal production), and supply raw materials for construction (13). The historical records document the practice of slash-and-burn agriculture by the first farmers (14–16). Forest areas were cut down and burned to produce charcoal, while the logged fields facilitated agriculture (14–16). The exploitation of the natural resources for local use and exportation leads to severe natural vegetation devastation. In the five centuries after the Portuguese settlement, more than 95% of Azorean natural vegetation has been destroyed (17). Currently, the vegetation of the Azores archipelago is highly degraded; lowland laurel forests are scarce and coastal woodlands are significantly reduced, and in most cases, invaded by exotic species, such as *Pittosporum undulatum* (18).

Lakes

The Azores are particularly rich in lentic habitats, with at least 88 lakes (19) located in five islands (São Miguel, Terceira, Pico and Flores and Corvo). Lakes in the Azores can be classified according to their geological setting into two main groups: (i) lakes within volcanic depressions and (ii) lakes in topographically depressed areas. The former are located in scoria cones, subsidence or collapsed calderas, or in maars. Typically, the lakes within the scoria cones are very small and shallow; lakes inside collapsed calderas show a larger surface area (Lake Azul, Lake Caldeirão), while those in maars are deeper (Lake Funda) (20). The studied lakes surface area ranges between 1.4 ha (Lake Ginjal in Terceira island) and 358.7 ha (Lake Azul in São Miguel island). Lake depth ranges between 0.5 m (Lake Ginjal) and 34.0 m depth (Lake Funda in Flores island). Lakes are located between 230 and 870 m of altitude. The Azorean lakes are subjected to several environmental pressures. Human colonization of the Azores, and the recent intensification of human activities within catchments (e.g., deforestation, agriculture, urbanization, and introduction of exotic species), has resulted in the eutrophication of many of the lakes (20–23). Azorean lakes have simple food webs and low diversity typical of remote island systems (24, 25). The natural features of these ecosystems and their small dimension within the Azorean archipelago increase its fragility and reduce the auto-regeneration ability. The main environmental gradient drivers for the biological assemblages are altitude, longitude, lake depth, and the lakes' trophic state (20, 21). Shallow lakes located at medium-high elevation (Lake Peixinho, Lake Caldeirão) are characterized by low conductivity and alkalinity, neutral to slightly acidic pH, and oligo-mesotrophic state (21). They have diverse phytoplankton communities but low biomass,

dominated by desmids, chlorophytes and chrysophytes (21). Diatoms are dominated by benthic and thycoplanktonic species belonging to the *Tabellaria*, *Brachysira*, *Encyonema* and *Frustulia* genera. The chironomid assemblages are dominated by *Micropsectra*, *Psectrocladius* and *Paratanytarsus* genus (20, 26). By contrast, deep lakes (Lake Azul, Lake Funda) are found at low elevations, present higher conductivity and alkalinity, and meso-eutrophic states (21). Phytoplankton communities present a low diversity with high biomass, dominated by cyanobacteria and diatoms. Besides the dominance of planktic diatoms (e.g., *Aulacoseira*, *Asterionella* and *Ulnaria* genera), a shift in benthic diatom assemblages towards the increase of *Achnantheidium*, *Pseudostaurosira*, *Nitzschia* and *Fragilaria* genera. Dominance of *Chironomus*, *Glyptotendipes* and *Psectrocladius* genera in the chironomid assemblages is also observed in deep lakes (20, 21, 26).

Methods

XRF core scanner

The better-preserved half of each section of the core was analyzed using X-ray fluorescence (XRF) with the AVAATECH XRF II core scanner at the Universitat de Barcelona (Spain). Depending on the main core lithological features, the XRF measurements were performed every 2 to 5 mm, where the material was well preserved (Table S1). Among the thirty-two chemical elements measured, we only employed the iron-manganese (Fe/Mn) ratio as an indicator of the lake bottom oxygenation conditions and titanium (Ti) as a proxy for the siliciclastic inputs due to runoff.

Organic matter

Organic matter content was analyzed for all lakes (Table S1). Samples for bulk organic geochemistry were 1 cm thick, and their sampling interval varied between 1 and 5 cm, depending on the temporal resolution of the record. They were manually ground using an agate mill and analyzed for Total Carbon (TC) and Total Nitrogen (TN) (Relative standard deviation (RSD) = 5 %), and their respective stable isotopes ($\delta^{13}\text{C}_{\text{org}}$ and $\delta^{15}\text{N}_{\text{org}}$) using a Finnigan delta Plus EA-CF-IRMS spectrometer at the Centres Científics i Tecnològics at Universitat de Barcelona (CCiTUB) and a Thermo Finnigan Flash- EA1112 elemental analyser at Servizo de Apoio á Investigación at Universidade da Coruña. Previous analyses by X-ray diffraction showed negligible amounts of carbonates; consequently, TC was considered to be equal to total organic carbon (TOC). TOC and TN results are expressed as percentages of the sediment dry weight. The atomic ratio TOC/TN was calculated and corrected according to (27) to discriminate inorganically bound nitrogen content from TN. Hereafter, the TOC/TN ratio is referred to as TOC/TN_{corr}. Isotopic values are reported in the conventional delta-notation (‰) relative to the Pee Dee Belemnite (PDB) carbon and atmospheric nitrogen (N₂) standards, respectively.

Palynological analyses

Palynological analyses were performed on all lake cores (Table S1). After spiking with *Lycopodium clavatum*, samples were digested with KOH, HCl, HF, and acetolysis. The residues were suspended in glycerine, and the microscopic slides were mounted in the same medium (28). Lake Azul samples were processed and analyzed at the Institute of Plant Science, University of Bern (Switzerland) and the Botanic Institute of Barcelona (IBB-CSIC, Spain), samples from Lakes Ginjal and Caldeirão were processed at the Universidade of the Azores (Portugal), and counted at the Universidade of the Azores (Portugal) and the University of Amsterdam (The Netherlands), respectively, and samples from Funda and Peixinho were processed and counted at Geosciences Barcelona (Geo3BCN-CSIC, Spain).

Identification of pollen, spores, and non-pollen palynomorphs (NPPs) was done at 400x magnification following (29–31), by comparison against the Azorean modern palynological library collection, curated by the Freshwater Ecology Research Group of the University of the Azores in Ponta Delgada, São Miguel. Non-pollen palynomorphs (NPP) were identified according to several specialized references (32–35). Cerealia were separated from the rest of the Poaceae based on the diameter of the pollen grain ($>47 \mu\text{m}$) and the annulus ($>11 \mu\text{m}$) (36). *Zea mays* and *Secale cereale* were identified according to Beug (37). Counting followed the criteria of Rull (38), ranging from 306 to 1051 (average 580) pollen grains and pteridophyte spores per sample. The pollen sum included all identified pollen and spore types with an ecological role in the landscape, except those from aquatic and semi-aquatic taxa (Cyperaceae, *Myriophyllum*, and *Potamogeton*). A detailed interpretation of the pollen diagram from Lake Azul can be found in (39).

Micro-charcoal particles were identified and counted on the same palynological slides according to two size classes between 5 – 40 μm and $> 40 \mu\text{m}$.

Plant macrofossils

Plant macrofossil analysis was only conducted on the Lake Caldeirão core (Table S1). The samples (5 cm^3) were gently washed using a sieve (125 μm mesh size) with 2 L of water. Sediment particles smaller than 125 μm were collected and left to decant in a container overnight. The screened material was transferred to Petri dishes, and plant macrofossils were separated under a stereomicroscope (10-50x). Moss leaves, Cyperaceae epidermal tissues, and small seeds were mounted into temporary slides and examined at high magnifications (100-400x). Identifications were made using a reference collection of plant parts and seed atlases (40–42) and illustrations in various publications (43–46). The macrofossil collection was stored in tubes with 70% ethanol at 4°C.

Macro-charcoal

Macroscopic charcoal analyses were conducted on contiguous 2 cm^3 sediment samples from Lakes Caldeirão, Peixinho, and Ginjal (Table S1). Samples were soaked in potassium hydroxide (KOH) solution (10 %) at 70°C for 30 minutes, then sieved to separate charcoal particles. These particles were counted in a Petri dish using a stereomicroscope. Charcoal concentrations (particles cm^{-3}) were converted to charcoal accumulation rates (CHAR, particles $\text{cm}^{-2} \text{yr}^{-1}$) by multiplying each concentration by the sediment accumulation rate (cm yr^{-1}).

Diatoms

Diatoms were identified and counted in all lake sediment cores (Table S1). Sediment samples were processed for diatoms following standardized procedures (47). The resulting slides were mounted with a Naphrax mountant, and at least 400 valves per sample were identified and counted across random transects at 1,000x magnification using a Zeiss Axio Imager A1 microscope equipped with a 100x objective (Zeiss Plan-Apo 1.4 numeric aperture) and differential interference contrast optics. Taxonomic identification was based on general diatom floras (48–54), and compared with previous studies in the Azores archipelago (55). Taxa were grouped according to their lifestyle preferences as euplanktonic, tychoplanktonic, and benthic (56). Diatoms with aerophilic capabilities (57) were considered distinct from benthic ones and categorized in their group. Raw valve counts were converted to percentage abundance data.

Chironomids

Head capsules (HC) of chironomid larvae were identified and counted in all lake sediment cores (Table S1). They were analyzed in 2 cm³ subsamples at 1 to 5 cm increments following the procedure described by (58). The samples were deflocculated in 10 % KOH, heated to 70 °C for 5 min, sieved and separated into two size fractions (90 and 212 μm). Head capsules were sorted under a stereomicroscope (40x magnification – Zeiss Stemi). HC were mounted with Euparal mounting medium and identified using a microscope at 100x – 400x magnification (ZEISS AXIOIMAGE A1). Identification of HC was mainly based on mentum characteristics, as described in (58), and were identified to the lowest possible taxonomic resolution, usually species morphotypes, using taxonomic nomenclature (58). The relative abundance of each taxon was presented as a percentage of the total chironomid count. Chironomids were grouped according to their habitat preference (profundal, littoral, sublittoral, or free-living taxa) or oxygen tolerance (low oxygen tolerance, stable oxygen, or unstable oxygen taxa). Each taxon was classified based on recent studies on chironomid autecology (see (59) and references therein).

Sterol determination

Sterols were measured in sediment samples from Lake Funda, Lake Peixinho, Lake Caldeirão, and Lake Azul (Table S1). Lipid analysis was carried out at the University of Texas (Lake Azul) and Brown University (Lakes Funda, Caldeirão and Peixinho).

All samples were freeze-dried and homogenized before solvent extraction using a Dionex accelerated solvent extraction (ASE 350) system at 120° C and 1200 psi with dichloromethane:methanol (DCM:MeOH; 9:1 v/v). The total lipid extract was separated using silica gel flash chromatography to obtain the alkane (hexane), ketone (DCM), and polar (MeOH) fractions. The resulting ketone fraction was analyzed for sterols, stanols, and polycyclic aromatic hydrocarbons (PAHs).

Sterol and stanol samples were identified and quantified using select ion monitoring with an Agilent 7890B gas chromatography (GC) system coupled to an Agilent 5977B quadrupole mass spectrometer (MS). The samples were injected onto a ZB-1MS (30 m x 320 μm x 0.25 μm) column in pulsed splitless mode (320 °C, 1.3 psi). The oven temperature was increased from 40° C for 1 min to 255° C at 20° C/min and further increased to 315° C at 4 °C/min where it was held isothermally for 10 min. The ionization energy for the MS was set to 70 eV and a scan range of 50-650 m/z was used. 5-cholestan-3-one was used as an internal standard.

PAHs were analyzed with an Agilent Technologies 1200 Series high-performance liquid chromatography (HPLC) system equipped with an autosampler, binary pump feeding into a reverse-phase liquid chromatography column, diode array detector (DAD), and fluorescence detector (FLD). Before analysis, all samples were filtered using an Agilent Captiva econofilter (2 μm mesh). PAH peaks were identified via the DAD UV spectra and were then quantified using the FLD. The FLD method was constructed based on previous HPLC analysis of PAHs in lake sediments. Varying PMT-Gain adjustments were made throughout the run to ensure the appropriate magnification of peaks in the final chromatograph. The results were analyzed on Chemstation using the LC 3Dsystems software. An external calibration curve was developed using an Accustandard PAH mix consisting of naphthalene, acenaphthene, fluorene, phenanthrene, anthracene, fluoranthene, pyrene, benz[a]anthracene, chrysene, benzo[b]fluoranthene, benzo[k]fluoranthene, benzo[a]pyrene, dibenzo[a,h]anthracene, benz[ghi]pyrene, and indeno[1,2,3-cd]pyrene with concentrations varying from 50 ng mL⁻¹ to 250 ng mL⁻¹. The resulting calibration curve was used to determine the final PAH concentrations.

Age-depth models for the sedimentary records

Samples for Radiocarbon AMS dating were prepared by acid digestion (60). Three plant macroremains (Lake Azul) and 40 pollen concentrated samples were analyzed at Beta Analytic Lab (USA) and Laboratoire de Radiochronologie (Université de Laval, Quebec, Canada). The

AMS radiocarbon dates (Table S2) were calibrated using the Calib 7.1 software and the IntCal20 calibration curve (61). The concentration profile of ^{210}Pb was determined every centimetre for the uppermost sediments of lakes Azul, Peixinho, Caldeirão, and Funda (Table S2) through quantification of ^{210}Po by alpha-particle spectrometry, at the Autonomous University of Barcelona (Lake Azul) following (62), and at the Laboratorio de Geoquímica Isotópica y Geocronología (Instituto de Ciencias del Mar y Limnología, UNAM, Mazatlán, México) following ((63), based on (64)). Briefly, aliquots of dried ground samples, ranging from 0.08 – 0.40 g, were spiked with a known amount of ^{209}Po yield tracer, digested with a mixture of concentrated acids ($\text{HF}+\text{HNO}_3+\text{HCl}$) at high temperature ($> 120^\circ\text{C}$), and polonium isotopes were spontaneously deposited on silver discs. ^{209}Po and ^{210}Po activities were determined by alpha-particle spectrometry with high-resolution low-background Si detectors until the counting uncertainty was estimated to be $< 5\%$. ^{226}Ra (via ^{214}Pb) and ^{137}Cs were determined by gamma spectrometry for selected samples along the cores from lakes Funda, Peixinho, and Azul (Table S1). About 1 g of dried ground sample was placed into polyethylene calibrated geometries (length = 40 mm, diameter = 10 mm) sealed with rubber caps and Teflon tape. Samples were stored for 21 days to allow secular equilibrium between ^{226}Ra and ^{214}Pb . Samples were measured in a gamma spectrometry system with a high-resolution low-background HPGe well-type detector (Ortec-Ametek) for at least 48 hours.

The excess ^{210}Pb activities were calculated by subtracting ^{226}Ra from the total ^{210}Pb activities. Activities are reported in Bq kg^{-1} and uncertainties are ± 1 sigma. Analytical quality was assured by replicate analysis of the reference material IAEA-300. Results were within the certified values for ^{210}Pb , ^{226}Ra and ^{137}Cs . $^{210}\text{Pb}_{\text{ex}}$ -derived sedimentation rates were calculated by applying the Constant Flux (CF; Azul) and the Constant Flux Constant Sedimentation (CF:CS; the other cores) models (65–67). Uncertainties were calculated using Monte-Carlo with 10,000 iterations (68).

In all cases, the combined age-depth model was constructed using version 2.3.9 of the R "clam" package (69, 70). This package automatically calibrated all radiocarbon dates at $2\text{-}\sigma$ using the IntCal20 calibration curve (61).

Climate Model Simulations

To investigate the climate conditions associated with land use changes and the occupation histories of our sites, we used the Community Earth System Model (CESM-CAM5_CN) Last Millennium Ensemble (LME) transient simulation. Ensemble members extend from 851 to 2006 CE and are forced using reconstructions of changing solar intensity, volcanic emissions, greenhouse gases, aerosols, land use conditions, and orbital parameters over this time interval. The transient simulations with CESM have been used previously in a number of experiments, ranging from an assessment of continental/oceanic changes associated with recent anthropogenic forcing (71, 72), to evaluating the relative roles of internal/external forcing and their impacts on global climate (73–75). These and other previous studies have demonstrated the model performance in reproducing large-scale circulation features such as the ones analyzed in this work (74, 76).

Data is available on a 2° horizontal resolution for atmospheric data, and 36 simulations were performed for the LME project: 13 simulations with all transient forcings, smaller ensembles with each transient forcing applied separately, and long 1850 and 850 CE control simulations. The Ensemble spread was generated by using round-off differences in the initial atmospheric state. The following variables were considered in this study: mean sea level pressure (MSLP), horizontal wind at the 925 hPa level (u and v), 2 m air temperature (T), and precipitation. Estimates of temperature and precipitation for the Azores were calculated using an average of the model output in the region between ($36^\circ\text{N} - 41^\circ\text{N}$) and ($32.5^\circ\text{W} - 22.5^\circ\text{W}$). Our analysis was restricted to simulations of the period from 851-2000 CE.

The monthly MSLP time series for the extended winter (October-March) season was used to calculate the following modes of atmospheric circulation: the North Atlantic Oscillation (NAO) and the Eastern Atlantic (EA) pattern. A classical approach based on MSLP dipoles was used to calculate the indices in this study. To compute the NAO, we considered the meridional difference in average MSLP between high-latitude [60° N-70° N / 30° W-10° W] and low latitude [30° N-40° N / 30° W-10° W] sectors in the North Atlantic. A similar approach was performed for the EA, in this case consisting of the zonal difference between a west [30° N-50° N / 50° W-30° W] east [30° N-50° N / 15° W-5° E] dipole in the northeastern Atlantic. Monthly anomalies were computed for the two dipoles relative to the 850-2000 CE climatological mean and then standardized to obtain a monthly NAO and EA series for the study period and each ensemble member. Monthly values not exceeding these thresholds were considered neutral. The typical individual and combined positive/negative anomalies in large-scale circulation and temperature (in the Euro-Atlantic sector) for NAO and EA phases during the 20th century were compared against the absolute average large-scale circulation during neutral phases, considering the Ensemble mean. Previous studies have used different definitions of the northern and southern components of the NAO and EA patterns, including station and areal averages as well as Principal Component Analysis (77, 78). Objective comparison of monthly and seasonal variability confirming the high level of similitude among these various definitions.

To obtain the combined phases of the circulation indices, we attributed positive (negative) phases of the modes when their values were above (below) 0.5 standard deviations of the series for the study period. For the analysis target period (851 – 1950 CE), the NAO and EA combinations were smoothed in time, using 10-, 30-, and 50-years filters to remove high-frequency variability and to obtain coherent circulation conditions at different time-scales. This was performed for each ensemble member.

Results

Sedimentary facies

Sediment cores were retrieved from five different lakes and the resulting composite cores vary in length and composition depending on the depositional environment and catchment area of the lake.

Lake Caldeirão

The sedimentary sequence from Lake Caldeirão (460 cm in length) is dominated by reddish-brown mud and plant fragments that were deposited under shallow lacustrine conditions. The mud facies overly thick tephra deposits (fine ash) that likely originated from cinder cones visible at the bottom of the present-day lake (Fig. S1).

Lake Funda

The sediment record from Lake Funda is 994 cm in length. The lower section of the core (368-994 cm) consists of brown to black organic-rich mud and plant remains that is interbedded with sand and gravel layers containing fragments of wood (Fig. S2). The uppermost section of the core (0-368 cm) is laminated with alternating layers of brown mud and yellow diatom oozes.

Lake Peixinho

The record retrieved from Lake Peixinho is 253 cm in length and overlies coarse-grained alluvial deposits. The lacustrine sediment is composed of massive brown to black mud and plant remains that were likely deposited under shallow lacustrine conditions (Fig. S3). Tephra layers (lapilli) were identified at 205-210 cm and 175-197 cm.

Lake Ginjal

The sediment core from Lake Ginjal (350 cm) consists of a tephra layer at 280-350 cm overlain by brown mud with plant remains in the uppermost 280 cm (Fig. S4).

Lake Azul

The original sediment record for Lake Azul was previously published and described in detail (39, 79). Briefly, the lowermost section of the core contains 2 m of compact, pumiceous, and gravelly tephra (lapilli). Between 116-150 cm the sediment is composed of alternating tephra deposits and silty-grey mud (Fig. S5). From 77-116 cm the sediment transitions to silty-brown mud that is rich in particles of volcanic glass. The uppermost 77 cm consist of brown mud interbedded with thin, turbidite-like layers that are rich in sand grains and terrestrial plant remains.

Record chronologies

All age-depth models were developed in R using the version 2.3.9 of the R Clam package (69, 70, 80). This package automatically calibrated all radiocarbon dates at 2- σ using the IntCal20 calibration curve (61).

Lake Caldeirão

The age-depth model was developed using nine ^{14}C dates (Table S2) and a ^{210}Pb profile that spans the uppermost 20 cm (Fig. S6). All samples were taken from the CL1703 core, except two samples at 110 cm and 190 cm depth that were taken from the CL19-02G gravity core, which was lithologically correlated to CL1703. The resulting age-depth model spans the last 4,000 years. The period from [500-1950 CE] studied in this manuscript has a sedimentation rate of ca. 0.6 mm yr^{-1} and the confidence interval for the Lake Caldeirão age-depth model ranges between 1.5 and 124 years.

Lake Funda

The age-depth model for Lake Funda was constructed using six ^{14}C dates (Table S2) and ^{210}Pb and ^{137}Cs profiles for the uppermost 74 cm (Fig. S4). Radiocarbon samples taken at 162, 168, 624 and 992 cm were discarded as they were located near allochthonous and coarse terrigenous sediments, resulting in the incorporation of old organic matter. The radiocarbon sample at 60.8 cm was also removed from the age-model as it was inconsistent with results from the ^{210}Pb and ^{137}Cs profiles. A linear interpolation was used to generate the age-depth model after removing slump events that were identified by coarse allochthonous and terrigenous material in the sediment record. The final age-depth model spans c. 720 years over 798 cm of sediment. The sedimentation rate decreases from ca. 7.3 mm yr^{-1} in the lower section of the sediment record (368-994 cm) to ca. 5.2 mm yr^{-1} in the uppermost section of the core (0-368 cm). The confidence interval for the Lake Funda age-depth model ranges between 1 and 50 years.

Lake Peixinho

For Lake Peixinho the age-depth model was developed with four ^{14}C dates (Table S2) and ^{210}Pb and ^{137}Cs profiles that span the uppermost 18 cm (Fig. S6). This model was constructed using a locally weighted spline (loess) with a smoothing factor of 0.1 after removing two lapilli tephra layers and a mass-wasting event between 18 and 47.5 cm. The radiocarbon date at 47.6 cm was removed from the final age-depth model due to its inconsistency with the ^{210}Pb dates and likely contamination from a mass-wasting event. The resulting age-depth model spans the last c. 690 years with sedimentation rates of 0.3 mm yr^{-1} from 216 to 212 cm, which increase to ca. 6 mm yr^{-1} on 205 cm and increase again to 7.9 mm yr^{-1} and 10.2 mm yr^{-1} 126 and 86 cm, respectively. The confidence interval for the Lake Peixinho age-depth model ranges between 1 and 112 years.

Lake Ginjal

The age-depth model for Lake Ginjal uses three ^{14}C dates and was generated using a smooth spline (Table S2; Fig. S6). Radiocarbon dates sampled at 40.0-42.5 and 237.5-240.0 cm were not included in the model because they were older than the stratigraphically adjacent dates. The resulting age-depth model spans c. 600 years from 1400-1950 CE with a sedimentation rate ranging from 25 mm yr^{-1} (275 cm) to 2.7 mm yr^{-1} (175 cm). The confidence interval for the Lake Ginjal age-depth model ranges between 10 and 110 years.

Lake Azul

The chronological model for Lake Azul was constructed using two ^{14}C dates and ^{210}Pb and ^{137}Cs profiles that span the uppermost 74 cm of the sediment record (Fig. S6). The age-depth model was previously published (39, 79) without the ^{210}Pb and ^{137}Cs data. Based on the ^{210}Pb profile from core AZ11-14, the previously published record from core AZ11-02 was missing the uppermost 19 cm and not 30 cm (79). The ^{14}C age at 82.8 cm was inconsistent with the results from the ^{210}Pb profile and therefore was excluded from the final age model. After removing four turbidite-like layers from the sediment record, the final age-depth model was constructed using a smooth spline method with 0.6 smoothing. The resulting age model spans the last ca. 700 years with a confidence interval for the age-depth model that ranges between 1.4 and 223 years.

Environmental and climatic evolution of Lakes Caldeirão, Funda, Peixinho, Ginjal, and Azul

Lake Caldeirão (Corvo Island)

Phase I (500-700 CE)

From 500-700 CE there are very few changes in the proxy-based records. About 85% of the pollen record is dominated by arboreal pollen and shrubs, particularly *Juniperus brevifolia*, *Ilex perado*, and *Myrsine africana* shrubs. The remaining pollen is derived from mosses and larger ferns (*Culcita macrocarpa* and *Dryopteris azorica*) (Fig. S1). A mean TOC/TN ratio of 18.4 ± 0.4 (Fig. S7A) and $\delta^{15}\text{N}$ values between 6.8 and 7.1 ‰, suggest that organic matter in the sediment record is primarily derived from allochthonous sources (81, 82). Ti values are lower in this section of the sediment record relative to Phases II and III (Fig. S1). Biological assemblages are dominated by benthic diatom taxa, such as *Staurosira* spp. and *Stauroforma* spp., and sublittoral and oligotrophic Chironomidae taxa (*Micropsectra* spp.), indicating low levels of productivity within the lake (83, 84). The Fe/Mn ratio also remains low, indicating that the lake bottom water remained oxic (85). Polycyclic aromatic hydrocarbons (PAHs), macro-charcoal particles (diameter $>125 \mu\text{m}$), spores from coprophilous fungi, and 5β -stigmastanol are largely absent in this section of the sediment record.

Phase II: 700 – 1070 CE

This period is marked by distinct changes in proxies derived from the terrestrial environment. First, with the increase of PAHs after c. 700 CE (total flux $< 6 \text{ ng cm}^{-2} \text{ yr}^{-1}$) and the first evidence of 5β -stigmastanol (total flux $< 2 \text{ ng cm}^{-2} \text{ yr}^{-1}$ around 750 CE and 820 CE). Macro-charcoal is present in the sediment record after c. 850 CE ($3.7 \text{ fragments cm}^{-2} \text{ yr}^{-1}$) and the first evidence of coprophilous fungi, around 880 CE. Although there are no major changes in the pollen record, the flux of *Juniperus* macrorests increases from 0.3 to 2.3 leaves $\text{cm}^{-2} \text{ yr}^{-1}$ after ca. 720 CE (Fig. S1). In contrast, there are no distinct changes in the macrophyte, diatom, and chironomid assemblages or in the bulk organic matter composition.

Phase III: 1070 – 1450 CE

The onset of this phase is marked by coincident increases in the sedimentation rate (ca. 11 mm yr⁻¹), 5 β -stigmastanol (0.14 $\mu\text{g cm}^{-2} \text{yr}^{-1}$), PAHs, and macro-charcoal (Fig. S1). This is followed by peaks in macro-charcoal particle inputs (maximum of 28.0 fragments cm⁻² yr⁻¹), PAH fluxes (increase from 3.0 $\times 10^5$ to 1.1 $\times 10^6$ ng cm⁻² yr⁻¹), *Juniperus* leaves (maximum value 35.1 leaves cm⁻² yr⁻¹), and macrophyte fluxes (maximum value 31.0 seeds cm⁻² yr⁻¹) ca. 1280 CE. These changes are followed by an increase in $\delta^{15}\text{N}$ 9.1 ‰, and a decrease in TOC/TN (from 19.3 to 15.9) around ca. 1280 CE. In the biological assemblages, aerophilic diatom taxa (*Humidophila* spp.: 16 %) increase and the unique occurrence of the planktonic *Fragilaria tenera* is observed. Similarly, the relative abundance of profundal chironomid taxa increases from 7.6 \pm 1.1 to 14.4 \pm 2.6 % (e.g. *Chironomus* spp.).

Phase IV: 1450 – 1950 CE

The beginning of this phase (ca. 1550 CE) is marked by a decrease of arboreal pollen from 27.1 to 17.8 %, an increase in macrophyte inputs (1.8 seeds cm⁻² yr⁻¹), and the disappearance of *Juniperus* leaves from the sediment record. Further, this time period is marked by the first appearance of *Aphanes*, an introduced plant species, in the pollen record. The chironomid assemblages also change ca. 1550 CE from sublittoral to predominantly littoral taxa. Coprophilous fungal spores also increase from 0.04 to 0.20 spores cm² yr⁻¹ after c. 1550 CE and the influx of 5 β -stigmastanol sporadically increases throughout this phase. TOC, TOC/TN, and $\delta^{13}\text{C}$ values increase throughout this phase, whereas $\delta^{15}\text{N}$ values decrease ca. 1680 CE from 7.6 to 4.7 ‰. In the diatom record, mesotrophic diatom species, such as *Nitzschia* spp., increase during this phase, whereas tychoplanktonic diatoms (i.e., *Staurosira* spp. and *Punctastriata* sp.) decrease. During this phase, we also observe opportunistic diatoms like *Achnanthydium minutissimum* (79).

Lake Funda (Flores Island)

Phase II: ca. 950 CE to 1070 CE

This section of the core is characterized by organic rich mud interbedded with gravel and sand layers (Fig. S2). The pollen record consists of about 75 % arboreal pollen, namely *Laurus azorica*, *Juniperus breviflora*, and *Picconia azorica*, and 10 % shrubs, including *Myrsine*, *Culcita macrocarpa*, and *Pteris incompleta*. Coprophilous fungal spores and 5 β -stigmastanol are absent in this section of the record. The TOC/TN ratio remains stable at 18.3 \pm 0.4, while $\delta^{15}\text{N}$ fluctuates between 2.6 and 6.3 ‰ (Fig. S2 and Fig. S7). The diatom assemblage is dominated by mesotrophic benthic taxa, such as *Navicula* spp. and *Psectrocladius* spp., and small tychoplanktonic diatom taxa (i.e., *Pseudostaurosira* spp. or *Staurosirella* spp.). Similarly, the chironomid assemblage primarily consists of species that are found in the profundal zone and tolerate low oxygen conditions, such as *Chironomus* spp.

Therefore, the changes in regional indicators, such as the large increase in micro-charcoal influx up to 3,024 particles cm⁻² yr⁻¹ ca. 1150 CE and the drop in arboreal pollen from 77.2 to 53.8 %, the rise of shrubs from 12.6 to 30.9 %.

Phase III: 1070 - 1450 CE

The onset of this phase is marked by the first appearance of coprophilous fungal spores (e.g., *Sporormiella*) ca. 1330 followed by a peak in macro-charcoal particles (840 \pm 48 particles cm² yr⁻¹) ca. 1400 CE and a decline in arboreal pollen from 75.2 \pm 2.1 to 54.9 \pm 9.3 % ca. 1420 CE (Fig. S2). The sedimentation rate increases from 9.4 \pm 0.8 to 12.2 \pm 1.0 mm yr⁻¹ at the start of this phase. This is followed by a rapid increase in the macrophyte influx with a maximum of 5022

seeds $\text{cm}^2 \text{yr}^{-1}$ ca. 1380 CE. These changes are coincident with a depletion of $\delta^{15}\text{N}$ from 3.8 ± 0.44 to 3.3 ± 0.2 ‰, a decrease in the TOC/TN ratio from 18.9 ± 0.4 to 12.9 ± 0.3 %, and a rise in mesotrophic and euplanktonic diatom species, namely *Aulacoseira granulata* and *Aulacoseira ambigua*. Further the abundance of chironomid head capsules, in particular macrophyte associated taxa, increases from 5.6 ± 1.0 to 9.9 ± 1.9 head capsules $\text{cm}^2 \text{yr}^{-1}$, whereas low oxygen tolerant taxa (*Chironomus* spp.) decrease.

Phase IV: 1450 CE to 1950 CE

The final phase is marked by a further decline in arboreal pollen from 37.5 to 29.6 % and the first detection of 5β -stigmastanol ($4.04 \mu\text{g cm}^2 \text{yr}^{-1}$) ca. 1500 CE. The influx of coprophilous fungal spores remains constant throughout this time period (mean value about 467 spores $\text{cm}^2 \text{yr}^{-1}$). This time period is also marked by the first appearance of coprostanol ca. 1625 CE in the sediment record. The sediment record also transitions from dark brown and organic rich mud to massive, brown and silty mud that is dominated by planktonic diatoms such as *Aulacoseira* spp. (>85 % of the diatom assemblage) ca. 1500 CE. $\delta^{15}\text{N}$ values also decline from 3.3 ± 0.2 to 2.0 ± 0.2 ‰, while Fe/Mn increases ca. 1600 CE. $\delta^{13}\text{C}$ values gradually decrease, whereas the TOC/TN ratio remains stable at 1700 CE.

Lake Peixinho (Pico Island)

Phase I (500-700 CE)

After ca. 690 CE, the pollen record shows a reduction in tree cover. The mean TOC/TN ratio remains around 18.6 ± 0.4 and $\delta^{15}\text{N}$ values remain around 2.8‰. The diatoms assemblage was dominated by oligotrophic benthic species, including the *Eunotia incisa* and *Eunotia rhomboidea* (79). The chironomid record was primarily composed of free-living chironomids, such as Tanypodinae (26, 83).

Phase II: 700 – 1070 CE

5β -stigmastanol was measured around ca. 700 CE. After c. 850 CE, 5β -stigmastanol and PAHs are continuously present in low abundance (Fig. S3) and coprostanol is absent. This is coincident with a small increase in macro-charcoal accumulation rates and a large, but brief, increase of allochthonous aerophilic diatoms (reaching 23.4 % of the diatom assemblage). This phase is also marked by the rise of mesotrophic tychoplanktonic diatoms, such as *Pseudostaurosira brevistriata*, and chironomids typically found in the profundal zone and under low oxygen conditions (e.g. *Chironomus* spp.). $\delta^{15}\text{N}$ values also decrease from 2.8 ± 0.4 to 1.9 ± 0.4 ‰.

Phase III: 1070 – 1450 CE

This phase is marked by the first occurrence of coprostanol ($0.01 \mu\text{g cm}^2 \text{yr}^{-1}$) ca. 1070 CE. The start of this phase is marked by a peak in 5β -stigmastanol ($0.17 \mu\text{g cm}^{-2} \text{yr}^{-1}$) and coprostanol ($0.04 \mu\text{g cm}^{-2} \text{yr}^{-1}$) at ca. 1120 CE (Fig. S3) and marked by the first evidence of coprophilous fungi. The initial increase in stanols is followed by a decrease in arboreal pollen from 77.1 to 54.0 % at ca. 1150 CE and a corresponding increase in the relative abundance of herbs from 19.0 to 34.5 %. After ca. 1330 CE the relative abundance of woody vegetation decreases again from 37.9 to 31.0 %, whereas herbaceous plants increase slightly from 53.9 to 56.3 %. A reappearance of *Secale cereale* occurs ca. 1200 CE, coinciding with an increase of *Plantago* spp. to 6.2 %. This phase is also associated with an increase in the sedimentation rate from 0.8 ± 0.1 to 3.3 ± 0.6 mm yr^{-1} . Macrocharcoal inputs to the sediment remain relatively low except for a small peak at ca. 1120 CE and a larger peak at ca. 1330 CE (15.7 particles $\text{cm}^2 \text{yr}^{-1}$). The flux of PAHs remains relatively constant (around $3 \mu\text{g cm}^2 \text{yr}^{-1}$) throughout this phase, except for two peaks at ca. 1120 CE ($7.18 \mu\text{g cm}^2 \text{yr}^{-1}$) and ca. 1330 CE ($8.64 \mu\text{g cm}^{-2} \text{yr}^{-1}$).

There are few changes in the diatom and chironomid assemblages between 1120 and 1330 CE. The relative abundance of aerophilic diatoms gradually increases during this phase, mainly associated with an increase in *Humidophila* spp. and *Karayevia* spp. After 1330 CE, however, there is an abrupt increase in meso-eutrophic planktonic diatoms, including *Aulacoseira* spp., and a decrease of free-living chironomids, namely *Tanypodinae* sp. In contrast, the macrophyte flux increases throughout this phase with a peak of 65.75×10^3 seeds $\text{cm}^{-2} \text{yr}^{-1}$ ca. 1330 CE. During this phase both TOC/TN and $\delta^{15}\text{N}$ values remain around constant at 14.7 ± 0.1 2.5 ± 0.3 ‰, respectively. Finally, there is an increase in Fe/Mn values from 80 to 164 throughout this phase.

Lake Ginjal (Terceira Island)

Phase IV: 1450 CE to 1950 CE

The pollen record is dominated by herbaceous plants (>90 %), namely *Poaceae* and *Plantago* spp., and a low abundance of pollen from trees (1.2 ± 0.3 %) and shrubs (5.0 ± 1.5 %) (Fig. S4). Native tree species are completely absent from this sedimentary sequence, whereas *Cerealia* sp. is detected in four different samples. Throughout this record the influx of coprophilous fungal spores (20.9 ± 14.3 spores $\text{cm}^{-2} \text{yr}^{-1}$) and macro-charcoal particles (15.5 fragments $\text{cm}^{-2} \text{yr}^{-1}$) remains elevated. The diatom assemblage includes aerophilic diatoms, such as *Pinnularia borealis* s.l., and diatoms found under eutrophic conditions like *Fragilaria tenera*. After c. 1450 CE there is a sharp increase in meso-eutrophic tycho planktonic diatoms, such as *Tabellaria flocculosa*, and in macrophyte associated taxa, such as *Paratanytarsus* sp. The chironomid assemblage is primarily composed of species found under low oxygen conditions (e.g. *Chironomus* spp.). The TOC/TN ratio remains low throughout this record (11.3 ± 0.05), whereas $\delta^{15}\text{N}$ gradually becomes more depleted, decreasing from 3.5 ± 0.3 to 2.1 ± 0.9 ‰ (Fig. S4 & S7d).

Lake Azul (São Miguel Island)

Phase III: 1280 – 1450 CE

The start of phase B in Lake Azul is marked by multiple tephra layers ca. 1280 CE (Fig. S5). These layers are followed by a sharp decline in aerophilic diatoms and a decline in Ti counts. The rest of phase B is dominated by benthic and opportunistic diatoms, including *Achnantheidium minutissimum* s.l. The pollen record is characterized by a decrease in arboreal pollen, in particular laurisilva, from ca. 60 to 20 % and an increase in pollen derived from shrubs. *Secale cereale* is also observed during this phase from ca. 1280-1350 CE. Coprophilous fungal spores, coprostanol, and 5β -stigmastanol are present throughout this record. This section of the sediment core also contains elevated charcoal counts, TOC/TN values around 8.8 ± 0.2 , and $\delta^{13}\text{C}$ values around -24.92 ± 1.98 ‰ (Fig. S7e).

Phase IV: 1450 CE to 1950 CE

Native shrubs and grasses dominate the pollen record during phase C, whereas only ca. 20% of the record is composed of arboreal pollen. TOC gradually increases from 0.61 to 1.43 % and TOC/TN values increase from 8.6 to 10.3. Both $\delta^{15}\text{N}$ and $\delta^{13}\text{C}$ becoming gradually more depleted during this phase with values decreasing from 2.5 to 1.2 ‰ and -24.1 to -25.6 ‰, respectively. In the diatom assemblage *Nitzschia* spp. and *Aulacoseira* spp. are both observed, which are found in under non-N limiting and eutrophic conditions, respectively (79).

Simulations

Simulations of Mean Sea Level Pressure (MSLP), 2 m temperature, and 925 hPa horizontal wind for combinations of NAO/EA phases during the period between 850-1950 CE (Fig. S8) display very similar results to the combinations of NAO/EA phases for the last century (Fig. S9).

Combined positive NAO and EA phases (Fig. S10) resulted in lower-than-average temperatures over Iceland, Greenland, and North Africa, whereas the United Kingdom, Scandinavia, and the eastern North Atlantic (including the Azores Archipelago) experienced higher-than-average temperatures. Two higher-than-normal MSLP centers were present over continental Europe and North America, and lower-than-average MSLP values occurred between 60 - 70 °N of the North Atlantic Ocean. This combination triggered wind field anomalies over the southeast and northwest Atlantic and a northernward migration of the westerlies.

Combined positive NAO and negative EA phases (Fig. S10) resulted in lower-than-average temperatures over Greenland, eastern North America, and the central Atlantic (45 – 60 °N by 15 – 45 °W). Conversely, Iceland, most of continental Europe, North Africa, and the mid-latitudes (30 – 45 °W) of the western Atlantic experienced higher-than-average temperatures. Low MSLP values occurred over Iceland and the British Isles, whereas high MSLP values were centered over the westernmost part of the Azores Archipelago. This atmospheric configuration resulted in enhanced westerly winds between 45 – 60 °N with a slightly enhanced northerly component.

Combined negative NAO and positive EA phases (Fig. S10) resulted in lower-than-average temperatures over eastern Europe and the mid-latitudes (30 – 45 °W) of the western Atlantic. In contrast, higher-than-average temperatures were observed over Greenland, eastern North America, and the central Atlantic. This NAO/EA combination triggered an MSLP dipole with higher-than-average MSLP values over Iceland and lower-than-average MSLP values over the central Atlantic. These MSLP anomalies gave rise to a southern migration of the westerlies (< 30 °N), resulting in weakened westerlies between 35 and 60 °N.

Combined negative NAO and EA phases (Fig. S10) resulted in lower-than-average temperatures over continental western and northern Europe and higher-than-average temperatures over the North Atlantic with maximum temperatures occurring in Iceland and Greenland. Similarly, MSLP anomalies were lower-than-average over Europe and higher-than-average over the North Atlantic. This pattern led to weakened westerly winds over the North Atlantic (25 – 65 °N) sector and enhanced northerly winds from Scandinavia to the Iberian Peninsula.

Phase II: 850- 1070 CE

Before ca. 900 CE, negative NAO phases were more frequent. During NAO⁻/EA⁺ and NAO⁻/EA⁻ phases temperatures were higher-than-average and lower-than-average, respectively, and the westerlies were weakened over the Azores Archipelago. Similar conditions occurred during NAO⁻/EA⁻ phases, but with an enhanced northerly wind over the Azores (Fig. S8 and Fig.S11).

Phase II roughly coincides with the Medieval Climate Anomaly (MCA), which is usually defined as a warmer-than-average period in the Northern Hemisphere (86). Our results from climate model simulations show higher-than-average temperatures at 900. Drier conditions occur in the Azores ca. 940-960 CE and 1070-1080 CE. Periods with prevalent NAO⁺/EA⁺ phases occurred at approximately 900, 950, 1030 CE, whereas NAO⁺/EA⁻ phases are observed at 930, 960, 1010, 1020 and 1070 CE. NAO⁻/EA⁻ phases are observed at 990-1000 CE (Fig. S8).

Phase III: 1070 – 1450 CE

Phase III corresponds to the transition between the MCA and the Little Ice Age (MCA-LIA) as well as the first 50 years of the LIA. The simulated precipitation suggests three cold events centered around 1180 CE, 1210 CE, between 1260 and 1300 CE; and that the Azores experienced wetter conditions between 1350-1450 CE. This coincides with a NAO⁺/EA⁻ phase between 1340-1380 CE, NAO⁻/EA⁺ phases at 1430-1460 CE and 1490 CE, and NAO⁻/EA⁻ phases at ca. 1110, 1180, 1210, 1270, 1420 and 1470 CE (Fig. S8). Between ca. 1430-1490 CE, temperatures dropped below average for this time period and NAO phases were more frequent. This was associated with weakened westerlies over the Azores Archipelago, and enhanced northerly winds during NAO⁻/EA⁻ phases.

Phase IV: > 1450 CE

Phase IV spans the LIA, which is usually defined by colder-than-average temperatures in the Northern Hemisphere. Results from the model simulations show that temperatures were above average between 1500-1600 CE and generally remained below average between 1600-1800 CE in the Azores Archipelago. Distinct cold periods are observed between 1700-1730 CE and 1750-1770 CE. There are few variations in the simulated precipitation with the exception of three dry intervals centered c. 1500-1520 CE, 1670-1690 CE, and 1770 CE. This is coincident with more frequent negative NAO phases. Positive EA phases dominate the 18th century, with a short interval of more frequent negative EA phases between c. 1720-1730 CE (Fig. S8).

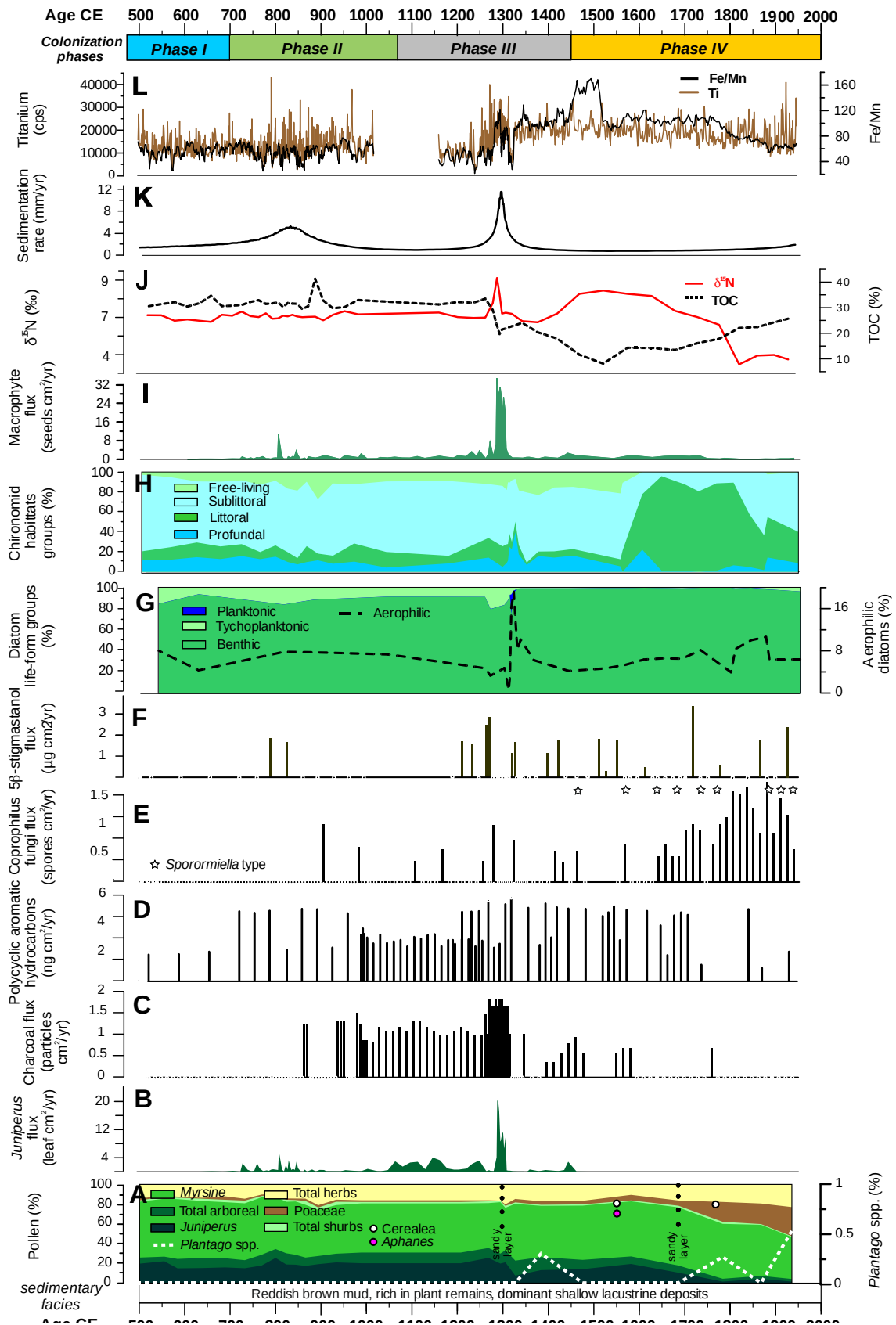


Fig. S1. Environmental evolution of Lake Caldeirão (Corvo Island) from 500 to 1950 CE. A) Pollen (%); B) Juniperus flux (leaf. $\text{cm}^{-2} \cdot \text{y}^{-1}$); C) Charcoal flux (particles. $\text{cm}^{-2} \cdot \text{y}^{-1}$); D) Total pyrolytic PAHs flux ($\text{ng} \cdot \text{cm}^{-2} \cdot \text{y}^{-1}$); E) Coprophilous fungi flux (spores. $\text{cm}^{-2} \cdot \text{y}^{-1}$); F) Fecal sterol biomarkers 5 β -stigmastanol flux ($\mu\text{g} \cdot \text{cm}^{-2} \cdot \text{y}^{-1}$) and coprostanol (5 β -cholestan-3 β -ol) G) Diatom life-forms groups (%) and aerophilic diatoms (%); H) Chironomid habitat associated (%) and chironomid head capsule flux ($\text{cm}^{-2} \cdot \text{y}^{-1}$); I) Macrophyte influx (seeds $\text{cm}^{-2} \cdot \text{y}^{-1}$) J) Nitrogen stable isotopes – $\delta^{15}\text{N}$ (‰) and Total organic content – TOC (%); K) sedimentation rate ($\text{mm}^{-1} \cdot \text{y}^{-1}$); L) Titantium (cps) and Fe/Mn ratio. Phases explanation (see main manuscript).

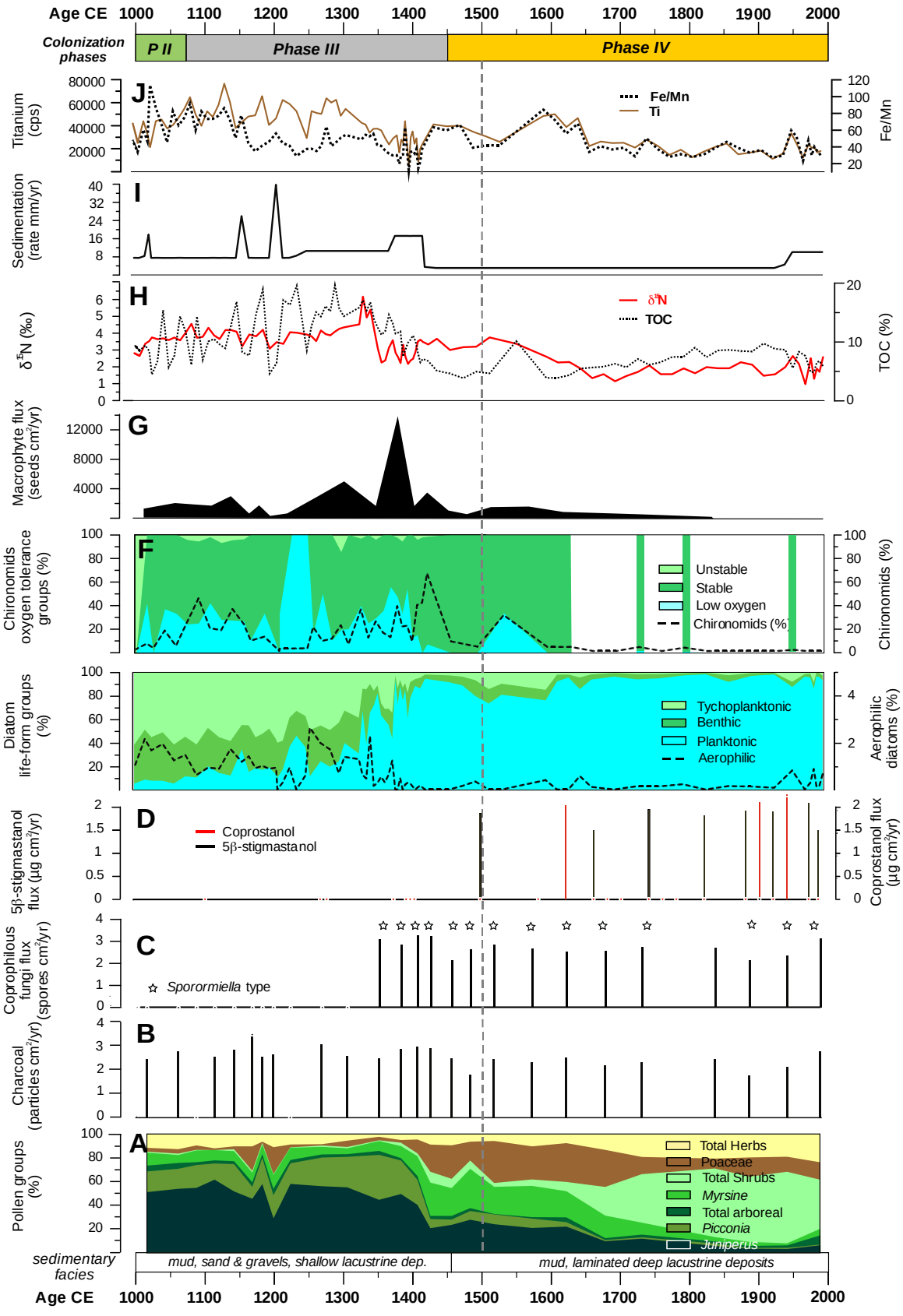


Fig. S2. Environmental evolution of Lake Funda (Flores Island) from 1000 to 1950CE. A) Pollen (%); B) Charcoal flux (particles. $\text{cm}^{-2}.\text{y}^{-1}$); C) Coprophilous fungi flux (spores. $\text{cm}^{-2}.\text{y}^{-1}$); D) Fecal sterol biomarkers 5β -stigmastanol flux ($\mu\text{g}.\text{cm}^{-2}.\text{y}^{-1}$) and coprostanol (5β -cholestan- 3β -ol) E) Diatom life-forms groups (%) and aerophilic diatoms (%), F) Chironomid habitat associated (%) and chironomid head capsule flux ($\text{cm}^{-2}.\text{y}^{-1}$); G) Macrophyte influx (seeds $\text{cm}^{-2}.\text{y}^{-1}$) H) Nitrogen stable isotopes – $\delta^{15}\text{N}$ (‰) and Total organic content – TOC (%); I) sedimentation rate ($\text{mm}^{-1}.\text{y}^{-1}$); J) Titanium (cps) and Fe/Mn ratio. Phases explanation (see main manuscript).

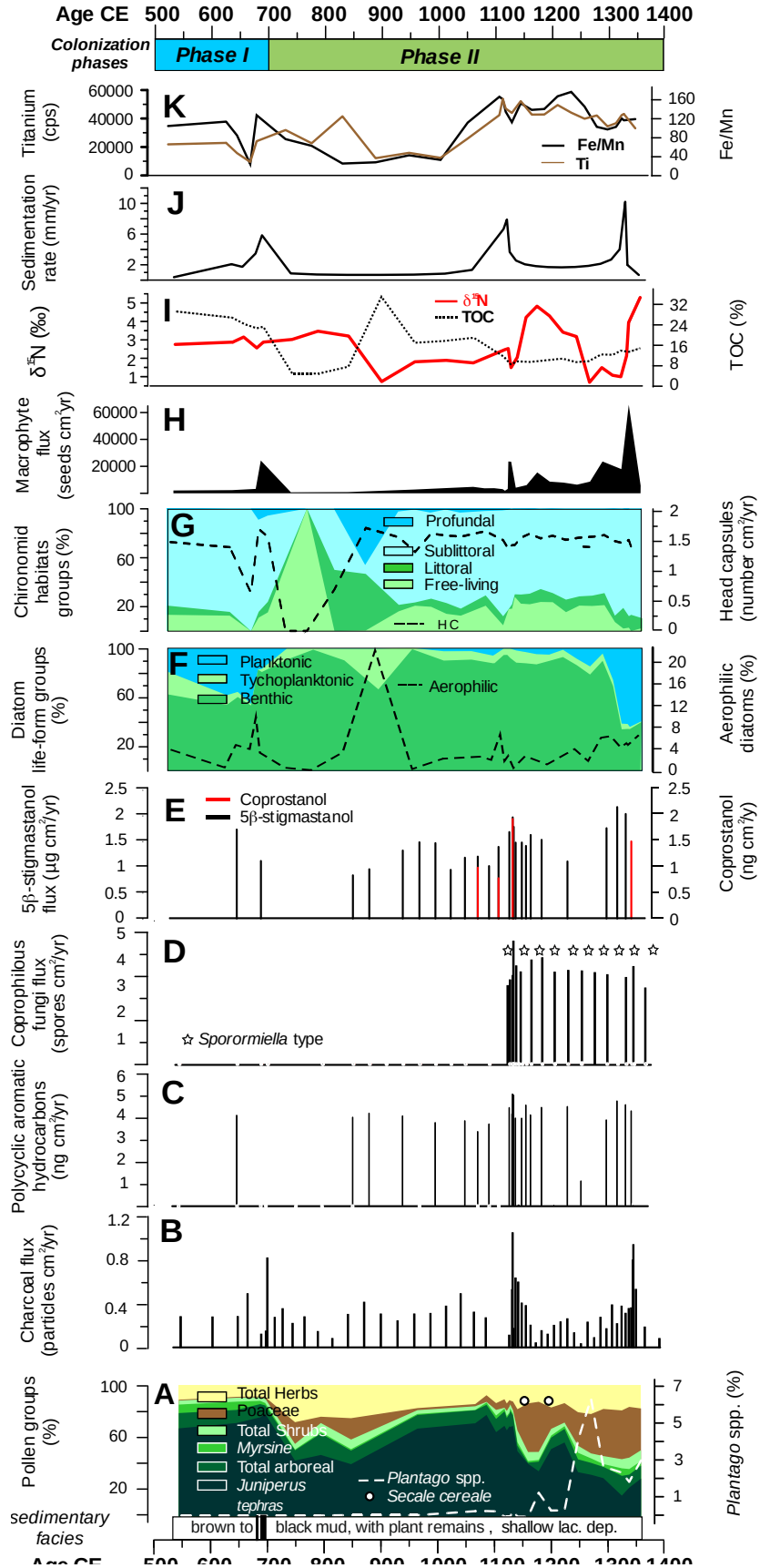


Fig. S3. Environmental evolution of Lake Peixinho (Pico Island) from 500 to 1800 CE. A) Pollen (%); B) Charcoal flux (particles. $\text{cm}^{-2}.\text{y}^{-1}$); C) Total pyrolytic PAHs flux ($\text{ng}.\text{cm}^{-2}.\text{y}^{-1}$); D) Coprophilous fungi flux (spores. $\text{cm}^{-2}.\text{y}^{-1}$); E) Fecal sterol biomarkers 5 β -stigmastanol flux ($\mu\text{g}.\text{cm}^{-2}.\text{y}^{-1}$) and coprostanol (5 β -cholestan-3 β -ol) F) Diatom life-forms groups (%) and Aerophilic diatoms (%); G) Chironomid habitat associated (%) and chironomid head capsule flux ($\text{cm}^{-2}.\text{y}^{-1}$); H) Macrophyte influx (seeds $\text{cm}^{-2}.\text{y}^{-1}$); I) Nitrogen stable isotopes – $\delta^{15}\text{N}$ (‰) and Total organic content – TOC (%); J) sedimentation rate ($\text{mm}^{-1}.\text{y}^{-1}$); K) Titanium (cps) and Fe/Mn ratio. Phases explanation (see main manuscript).

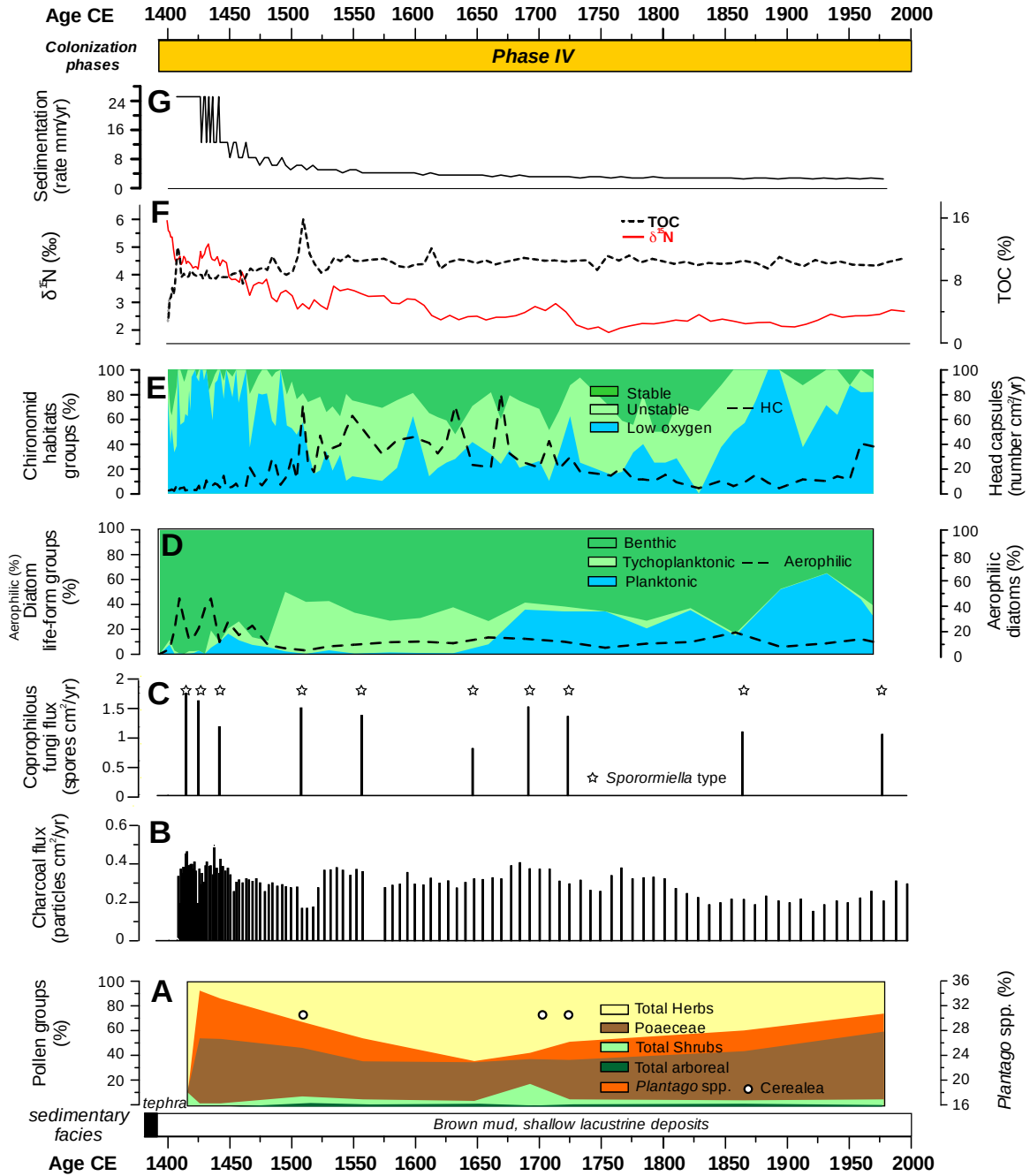


Fig. S4. Environmental evolution of Lake Ginjal (Terceira Island) from 1400 to 1800 CE. A) Pollen (%) and *Plantago* spp. (%); B) Charcoal flux (particles. $\text{cm}^{-2}.\text{y}^{-1}$); C) Coprophilous fungi flux (spores. $\text{cm}^{-2}.\text{y}^{-1}$); D) Diatom life-forms groups (%) and aerophilic diatoms (%), E) Chironomid habitat associated (%) and chironomid head capsule flux ($\text{cm}^{-2}.\text{y}^{-1}$); F) Nitrogen stable isotopes – $\delta^{15}\text{N}$ (‰) and Total organic content – TOC (%); G) Sedimentation rate ($\text{mm}^{-1}.\text{y}^{-1}$). Phases explanation (see main manuscript).

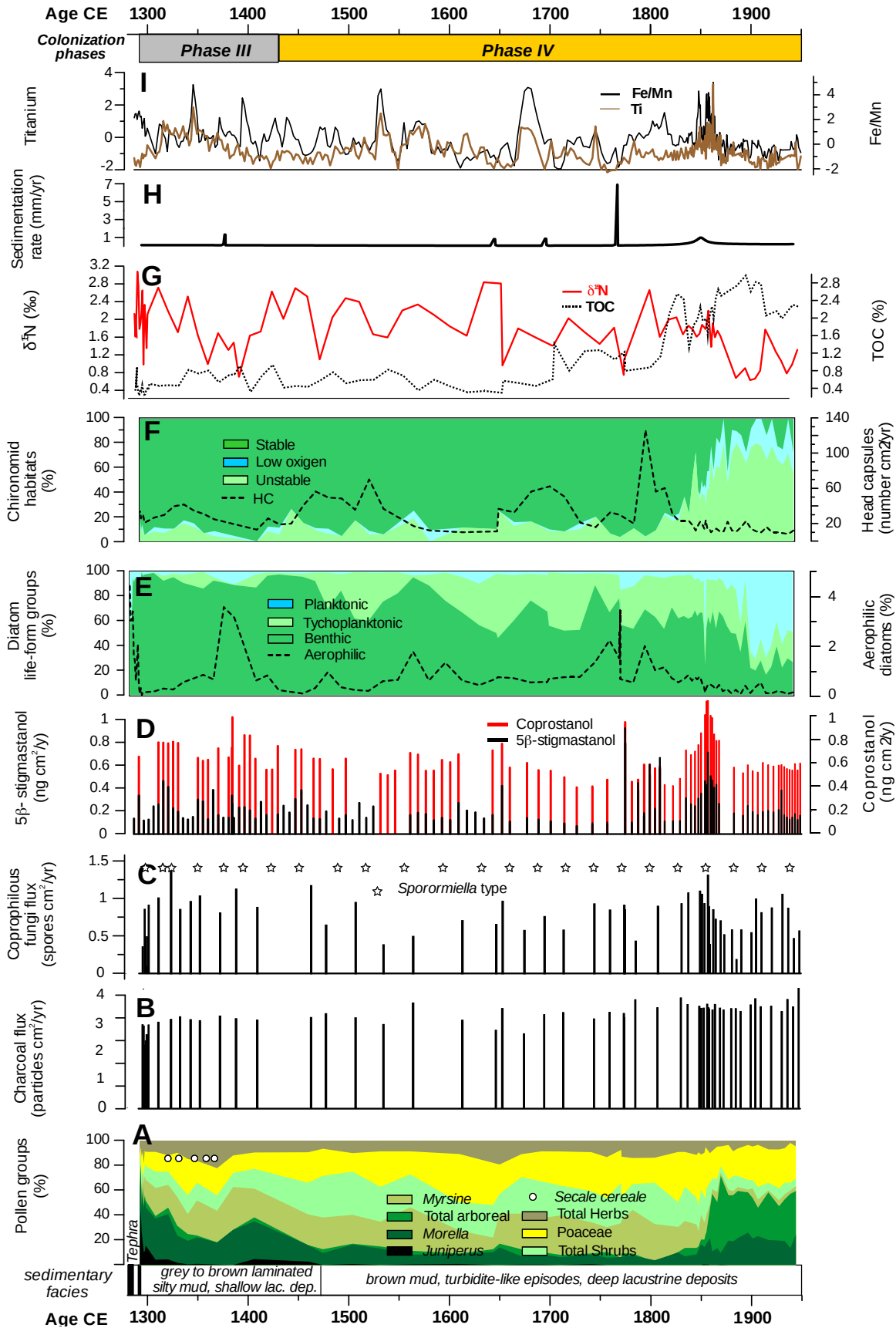


Fig. S5. Environmental evolution of Lake Azul (São Miguel Island) from 1280 to 1800 CE. A) Pollen (%); B) Charcoal flux (particles. $\text{cm}^{-2}.\text{y}^{-1}$); C) Coprophilous fungi flux (spores. $\text{cm}^{-2}.\text{y}^{-1}$); D) Fecal sterol biomarkers 5β -stigmastanol flux ($\text{ng}.\text{cm}^{-2}.\text{y}^{-1}$) and coprostanol (5β -cholestan- 3β -ol) E) Diatom life-forms groups (%) and aerophilic diatoms (%); F) Chironomid habitat associated (%) and chironomid head capsule flux ($\text{cm}^{-2}.\text{y}^{-1}$); G) Nitrogen stable isotopes – $\delta^{15}\text{N}$ (‰) and Total organic content – TOC (%); H) Sedimentation rate ($\text{mm}^{-1}.\text{y}^{-1}$); I) Titanium (cps) and Fe/Mn ratio. Phases explanation (see main manuscript).

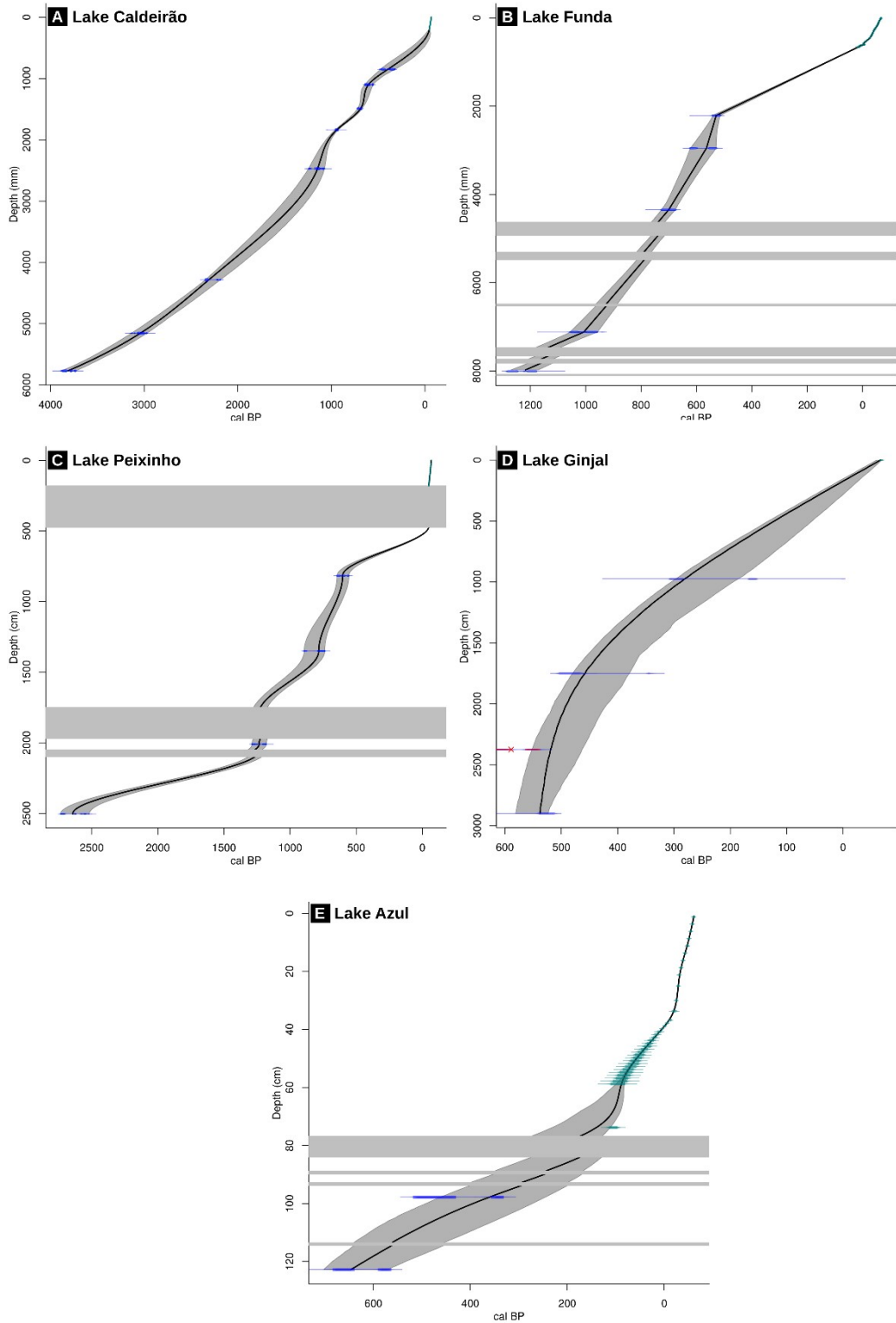


Fig. S6. Age-depth models of Lakes Caldeirão (A – top left), Funda (B – top right), Peixinho (C – middle left), Ginjal (D – middle right), and Azul (E – bottom center). All models were built using the R clam package version 2.3.9 (Blaauw, 2021), which uses the latest Intcal20 calibration curve. Horizontal gray bands denote the stratigraphic position of both instantaneous flood events (Lakes Azul, Funda, and the uppermost event of Peixinho) and volcanic tephras (lower two bands of Lake Peixinho). In green, the samples whose age was derived from the ^{210}Pb and ^{137}Cs profiles, in blue the radiocarbon dates used in the age-depth model construction, and in red the radiocarbon dates discarded. The confidence interval for the Lake Caldeirao age-depth model ranges between 1.5 and 124 years while for Lake Funda oscillates between 1 and 50 years, for Lake Peixinho fluctuates between 1 and 110 years, for Lake Ginja between 10 and 112 years, and finally, for Lake Azul between 1.4 and 223 years. Radiocarbon results employed to build these chronological models are in Table S2. Some radiocarbon dates were finally excluded of the final age-depth models due to inconsistent results. Most of these inconsistencies were related to the proximity of the dated material to allochthonous coarse terrigenous sediments (see the Records chronology section for further details).

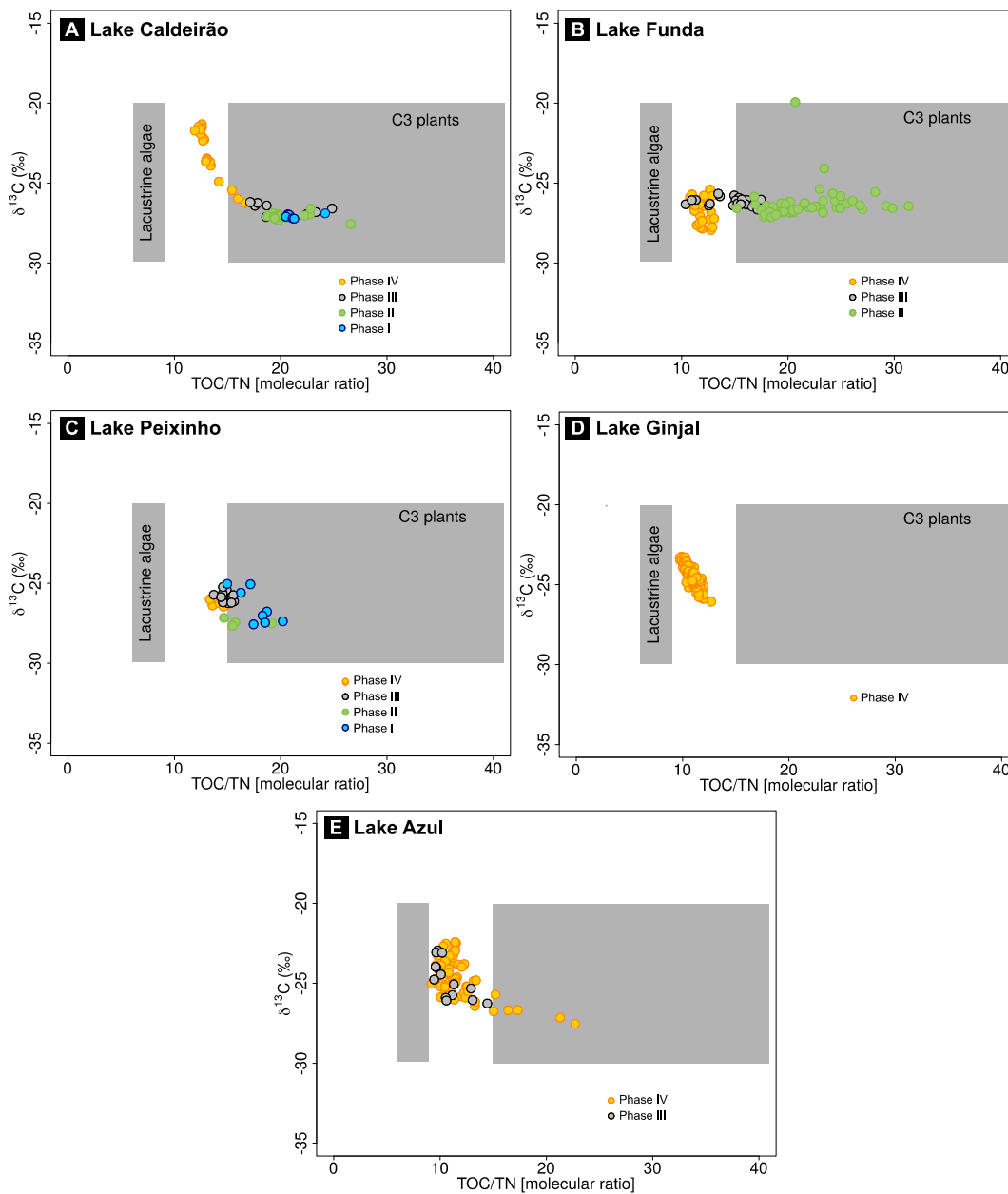


Fig. S7. Change in bulk organic matter content according to the three defined phases of anthropogenic impact compared to the "Pre-settlement phase". Western group A) Lake Caldeirão (Corvo Island); B) Lake Funda (Flores Island); Central group C) Lake Peixinho (Pico Island); D) Lake Ginjal (Terceira Island) and Eastern group E) Lake Azul (São Miguel Island). Changes in TOC/TN were interpreted in terms of allochthonous (vegetal cover debris) versus autochthonous (algal in-lake) sources while $\delta^{13}\text{C}$ was employed as one of the lake trophic status indicator (See the detailed climate and environmental reconstructions of the five lakes explained in the section "Environmental and climatic evolution of Lakes Caldeirão, Funda, Peixinho, Ginjal, and Azul" for further details).

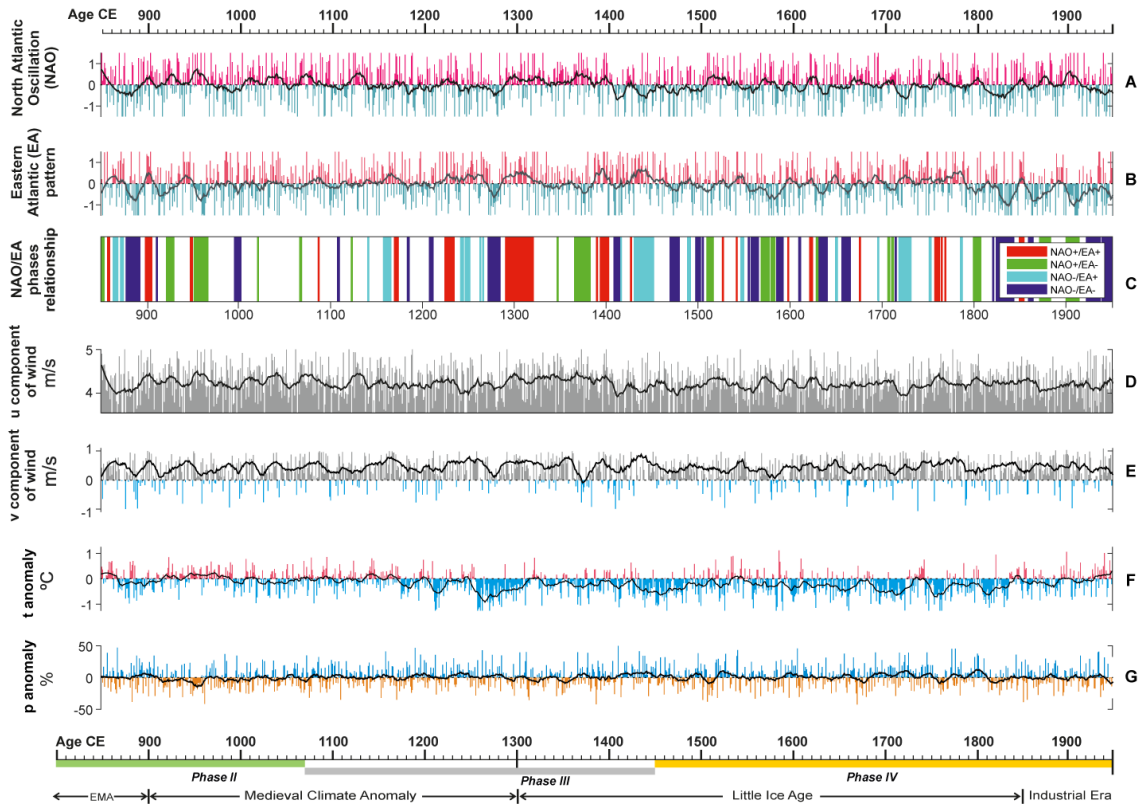


Fig. S8. (a) Extended winter (Oct-Mar) simulated NAO values between 850 and 1950 CE. The black line indicates a 30-year smoothing filter. (b) Extended winter simulated EA values between 850 and 1950 CE. The black line indicates a 30-year smoothing filter. (c) 30-years combinations of NAO and EA. (d) Extended winter simulated U-wind component between 850 and 1950 CE for the Azores Archipelago ($0.95^{\circ} \times 1.25^{\circ}$ grid). The black line indicates a 30-year smoothing filter. (e) Extended winter simulated V-wind component anomalies (computed for 850-1950 CE) between 850 and 1450 CE for the Azores Archipelago ($0.95^{\circ} \times 1.25^{\circ}$ grid). The black line indicates a 30-year smoothing filter. (f) Extended winter simulated temperature anomalies (computed for 850-1800 CE) between 850 and 1950 CE for the Azores Archipelago ($0.95^{\circ} \times 1.25^{\circ}$ grid). The black line indicates a 30-year smoothing filter. (g) Extended winter simulated precipitation anomalies (computed for 850-1950 CE) between 850 and 1950 CE for the Azores Archipelago ($0.95^{\circ} \times 1.25^{\circ}$ grid). The black line indicates a 30-year smoothing filter. Note that human activity phases and main North Atlantic climatic stages are indicated in the bottom timeline.

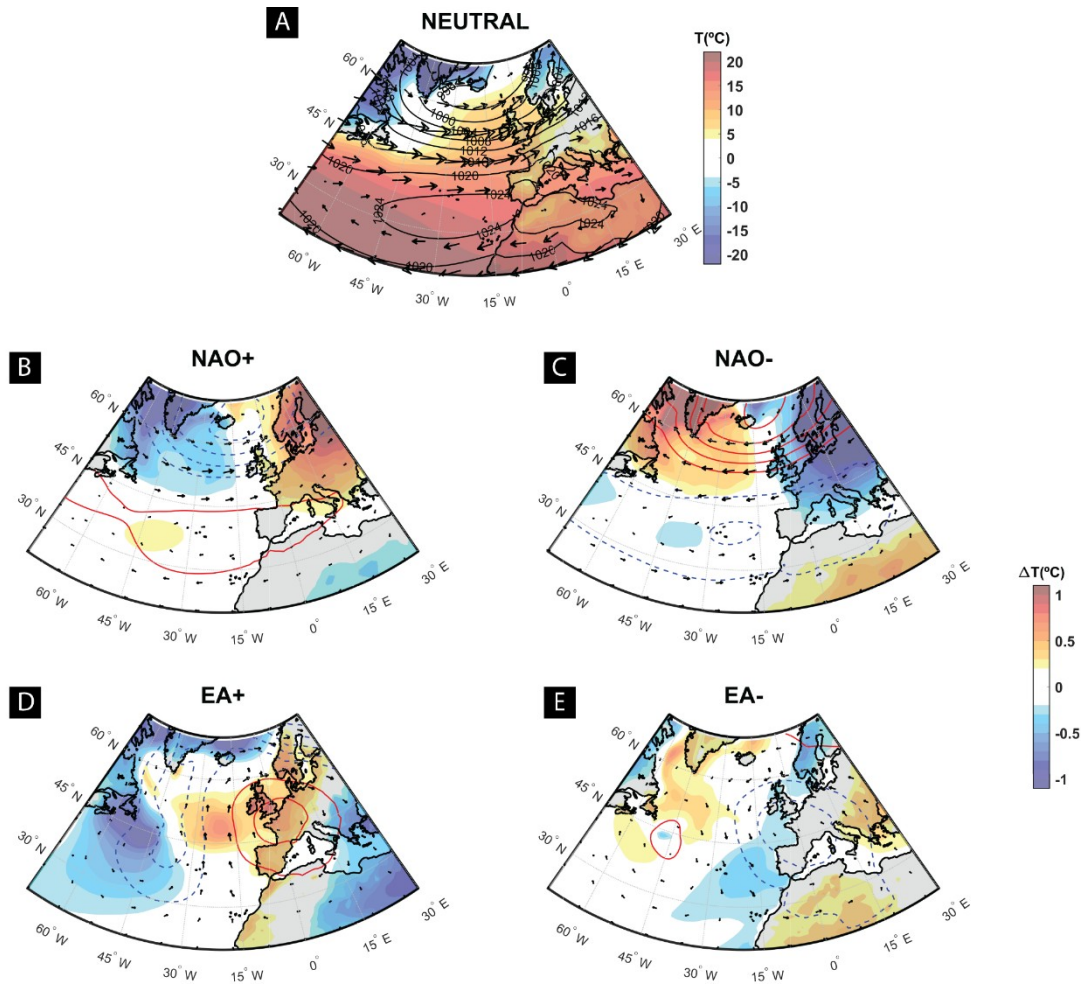


Fig. S9. Average anomalies for MSLP (blue/red lines), 2 m temperature (shading), and 925 hPa horizontal wind (vectors) for the combinations between concurrent positive/negative phases of the NAO and EA during 1901-2000 extended winters (October-March). (a) positive NAO and EA. (b) positive NAO and negative EA. (c) negative NAO and positive EA. (d) negative NAO and EA.

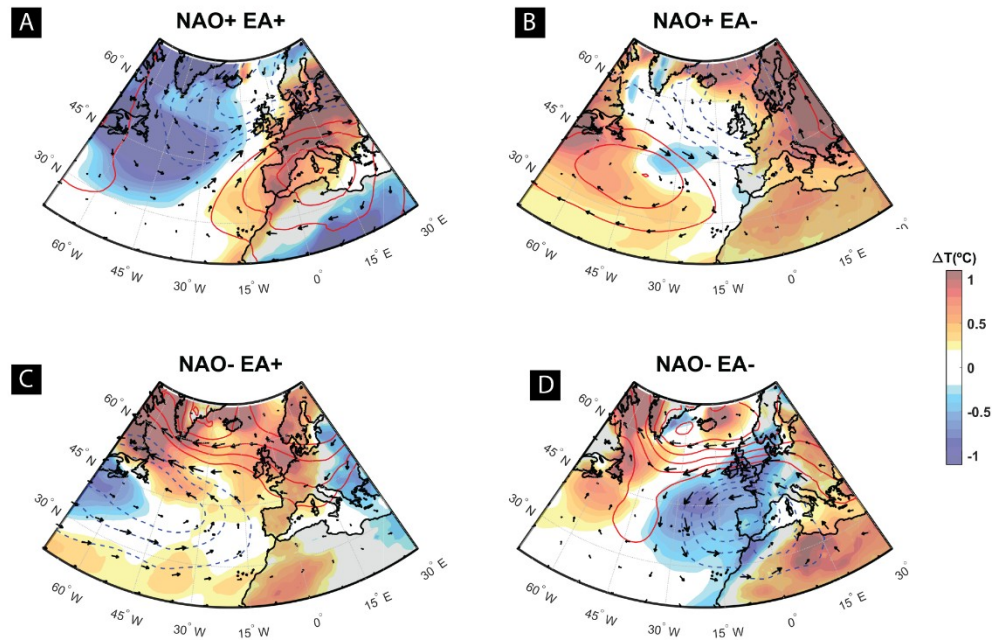


Fig. S10. Average anomalies for MSLP (blue/red lines), 2 m temperature (shading), and 925 hPa horizontal wind (vectors) for the combinations between concurrent positive/negative phases of the NAO and EA during 1901-2000 extended winters (October-March). (a) positive NAO and EA. (b) positive NAO and negative EA. (c) negative NAO and positive EA. (d) negative NAO and EA.

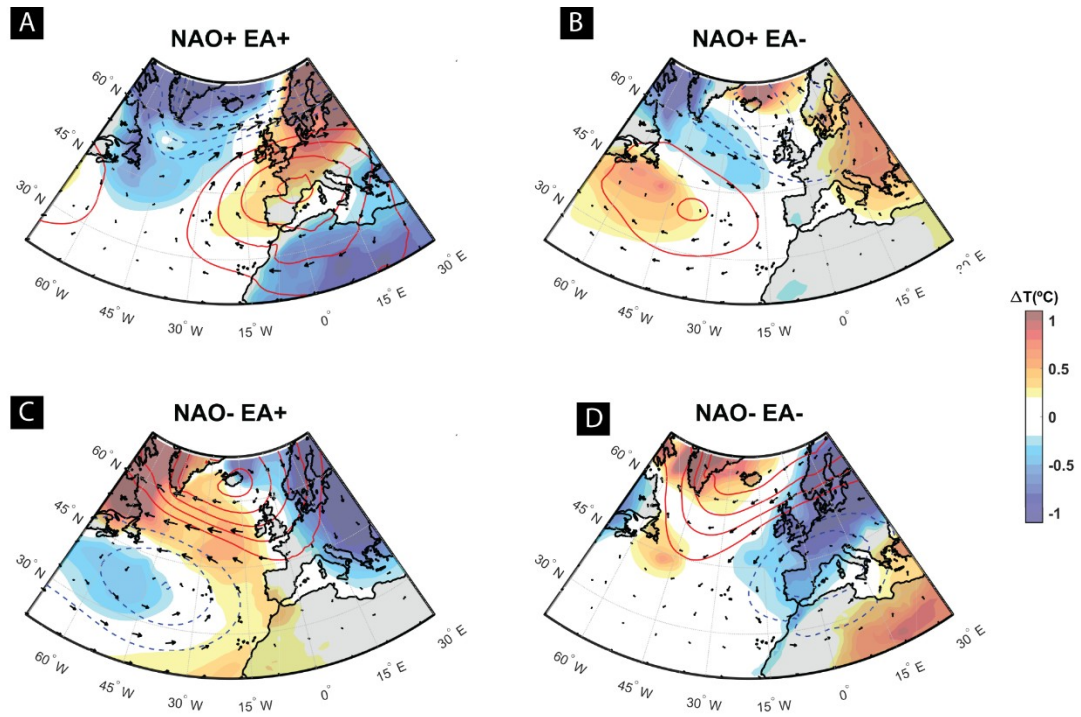


Fig. S11. Average anomalies for MSLP (blue/red lines), 2 m temperature (shading), and 925 hPa horizontal wind (vectors), for the combinations between concurrent positive/negative phases of the NAO and EA during 850 – 1450 CE period. (a) positive NAO and EA. (b) positive NAO and negative EA. (c) negative NAO and positive EA. (d) negative NAO and EA.

Tables

Table S1. Summary of the studied proxies and their sampling resolution in millimetres (mm) per lake. (–) indicates proxy method not used on a core and (X) indicates use of this dating method on a core.

Proxy Lake	Lake Funda	Lake Peixinho	Lake Ginjal	Lake Caldeirão	Lake Azul
X-Ray Fluorescence (XRF)	2	2	–	2	2
Bulk organic matter	50	40	25	50	10
Pollen	50-100	40-80	50	100	20
Plant macrorests	–	–	–	20	–
Macro-charcoal	–	40	25	50	–
Diatoms	100	40	20	50	20
Chironomids	100	40	20	50	10
Sterols	50	40	20	50	5
¹⁴ C AMS dates	X	X	X	X	X
²¹⁰ Pb profile	X	X	–	X	X
¹³⁷ Cs profile	X	X	–	–	X

Table S2. Radiocarbon dates of the sedimentary sequences, including laboratory code (UCIAMS- University of California; ULA – University of Laval and Beta – Beta Analytic), sample description, sample ID, collected depth (cm), pre-treatment, fraction modern values F14C, per mil depletion or enrichment D14C, uncalibrated 14C ages and 14C calibrated ages

Laboratory code	Sample description	Sample ID	Depth (cm)	Pre-treatment	F ¹⁴ C	D ¹⁴ C	¹⁴ C age (yrs BP)	2-σ cal. ¹⁴ C age (yrs BP)	
Lake Caldeirão (Corvo Island)									
UCIAMS-203216	ULA 7752	Pollen concentrate	CL1703-01-78	85	HCl	0.9573 ± 0.0023	-42.7 ± 2.3	350 ± 20	390 ⁺¹⁰ ₋₇₀
UCIAMS-230042	ULA-8880	Pollen concentrate	CL19-02G	110	HCl-NaOH-HCl	0.9277 ± 0.0015	-72.3 ± 1.5	605 ± 15	604 ⁺⁴⁰ ₋₂₀
UCIAMS-212644	ULA-8250	Pollen concentrate	CL1703-01-149	149	HCl	0.9089 ± 0.0015	-91.1 ± 1.5	765 ± 15	688 ⁺²⁰ ₋₂₀
UCIAMS-230043	ULA-8881	Pollen concentrate	CL19-02G	190	HCl-NaOH-HCl	0.8705 ± 0.0015	-129.5 ± 1.5	1115 ± 15	1015 ⁺⁴⁵ ₋₄₀
UCIAMS-203215	ULA-7751	Pollen concentrate	CL1703-02-65	247	HCl-NaOH-HCl	0.8586 ± 0.0018	-141.4 ± 1.8	1225 ± 20	1150 ⁺³⁰ ₋₈₀
UCIAMS-215536	ULA-8356	Pollen concentrate	CL1703-03-66	428.4	HCl-NaOH-HCl	0.7517 ± 0.0014	-248.3 ± 1.4	2295 ± 20	2335 ⁺¹⁵ ₋₂₅
UCIAMS-215537	ULA-8357	Pollen concentrate	CL1703-03-144	515.5	HCl-NaOH-HCl	0.6966 ± 0.0012	-303.4 ± 1.2	2905 ± 15	3035 ⁺⁴⁰ ₋₇₀
UCIAMS-203208	ULA-7750	Pollen concentrate	CL1703-04-28	577	HCl-NaOH-HCl	0.6437 ± 0.015	-356.3 ± 1.5	3540 ± 20	3840 ⁺⁵⁰ ₋₂₀
Lake Funda (Flores Island)									
UCIAMS-203206	ULA-7746	Pollen concentrate	FN1702-01-52.8	60.8	HCl-NaOH-HCl	1.0097 ± 0.0025	9.7 ± 2.5	Modern	1955.6 ^{+0.3} _{-0.3}
UCIAMS-170194	ULA-5787	Pollen concentrate	FN1702-01-154	162	none	0.9363 ± 0.0017	-63.7 ± 1.7	530 ± 15	537 ⁺¹⁰ ₋₁₀
UCIAMS-203213	ULA-7747	Pollen concentrate	FN1702-01-160	168	HCl-NaOH-HCl	0.8359 ± 0.0019	-164.1 ± 1.9	1440 ± 20	1330 ⁺⁴⁰ ₋₃₀
UCIAMS-200963	ULA-7657	Pollen concentrate	FN1702-02-34	221.2	HCl-NaOH-HCl	0.9385 ± 0.0017	-61.5 ± 1.7	510 ± 15	530 ⁺¹⁰ ₋₁₀
UCIAMS-203205	ULA-7745	Pollen concentrate	FN1702-02-108	295.2	HCl-NaOH-HCl	0.9338 ± 0.0022	-66.2 ± 2.2	550 ± 20	550 ⁺⁸⁰ ₋₅₀
UCIAMS-203204	ULA-7744	Pollen concentrate	FN1702-03-67	435	HCl-NaOH-HCl	0.9067 ± 0.0022	-93.3 ± 2.2	785 ± 20	700 ⁺³⁰ ₋₂₀
UCIAMS-203202	ULA-7738	Pollen concentrate	FN1702-04-47	624	HCl-NaOH-HCl	0.8461 ± 0.0020	-153.9 ± 2.0	1340 ± 20	1280 ⁺²⁰ ₋₂₀
UCIAMS-203203	ULA-7739	Pollen concentrate	FN1702-04-135	712	HCl-NaOH-HCl	0.8722 ± 0.0020	-127.8 ± 2.0	1100 ± 20	1000 ⁺⁶⁰ ₋₄₀
UCIAMS-203201	ULA-7737	Pollen concentrate	FN1702-05-73	801	HCl-NaOH-HCl	0.8508 ± 0.0020	-149.2 ± 2.0	1300 ± 20	1250 ⁺⁴⁰ ₋₂₀
UCIAMS-200961	ULA-7655	Pollen concentrate	FN1702-06-71	992	HCl-NaOH-HCl	0.8834 ± 0.0018	-116.6 ± 1.8	995 ± 20	930 ⁺³⁰ ₋₃₀
Lake Peixinho (Pico Island)									
UCIAMS-167858	ULA-5708	Pollen concentrate	PEX171B-01-36	47.6	HCl	0.9454 ± 0.0018	-54.6 ± 1.8	450 ± 20	510 ⁺²⁰ ₋₂₀

UCIAMS-167856	ULA-5705	Pollen concentrate	PEX171A-01-81	81.7	none	0.9264 ± 0.0021	-73.6 ± 2.1	615 ± 20	600 +50 -10
UCIAMS-170195	ULA-5788	Pollen concentrate	PEX171A-01-135	135	none	0.8950 ± 0.0016	-105.0 ± 1.6	890 ± 15	790 +10 -50
UCIAMS-167857	ULA-5707	Pollen concentrate	PEX171Csup-53	201	none	0.8491 ± 0.0021	-150.9 ± 2.1	1315 ± 20	1270 +20 -30
UCIAMS-167869	ULA-5719	Pollen concentrate	PEX171Csup-104	250.4	HCl	0.7288 ± 0.0017	-271.2 ± 1.7	2540 ± 20	2715 +30 -20
Lake Ginjal (Terceira Island)									
UCIAMS-215539	ULA-8359	Pollen concentrate	GN-01 M1 40	41.2	HCl	0.9653 ± 0.0017	-34.7 ± 1.7	285 ± 15	385 +50 -5
UCIAMS-211262	ULA-8211	Pollen concentrate	GW-01-02 47.5-50	97.5	HCl	0.9698 ± 0.0017	-30.2 ± 1.7	245 ± 15	295 +10 -10
UCIAMS-211261	ULA-8210	Pollen concentrate	GW-01-04 25-27.5	175	none	0.9516 ± 0.0020	-48.4 ± 2.0	400 ± 20	485 +25 -35
UCIAMS-211263	ULA-8212	Pollen concentrate	GW-01-05 37.5-40	275	HCl	0.9306 ± 0.0021	-69.4 ± 2.1	580 ± 20	610 +30 -20
UCIAMS-215540	ULA-8360	Pollen concentrate	GN M6 25 290	238.2	HCl-NaOH-HCl	0.9392 ± 0.0016	-60.8 ± 1.6	505 ± 15	530 +10 -20
Lake Azul (São Miguel Island)									
Beta-316595		Macrorest	AZ11-02-46	82.8	alkali	-	-	200 ± 30	180 +40 -40
Beta-331408		Macrorest	AZ11-02-61	97.8	alkali	-	-	420 ± 30	490 +30 -55
Beta-331409		Macrorest	AZ11-02-86	122.8	alkali	-	-	690 ± 30	660 +20 -20

SI References

1. R. S. Ramalho, *et al.*, Emergence and evolution of Santa Maria Island (azores)- The conundrum of uplifted islands revisited. *Bull. Geol. Soc. Am.* **129**, 372–391 (2017).
2. A. C. G. Costa, A. Hildenbrand, F. O. Marques, A. L. R. Sibrant, A. Santos de Campos, Catastrophic flank collapses and slumping in Pico Island during the last 130 kyr (Pico-Faial ridge, Azores Triple Junction). *J. Volcanol. Geotherm. Res.* **302**, 33–46 (2015).
3. A. Hernández, *et al.*, The influences of the AMO and NAO on the sedimentary infill in an Azores Archipelago lake since ca. 1350 CE. *Glob. Planet. Change* **154**, 61–74 (2017).
4. A. Hernández, *et al.*, New Azores archipelago daily precipitation dataset and its links with large-scale modes of climate variability. *Int. J. Climatol.* **36**, 4439–4454 (2016).
5. D. L. Volkov, L. Fu, On the Reasons for the Formation and Variability of the Azores Current. *J. Phys. Oceanogr.* **40**, 2197–2220 (2010).
6. J. W. Hurrell, Y. Kushnir, G. Ottersen, M. Visbeck, An Overview of the North Atlantic Oscillation. *North Atl. Oscil. Clim. Significance Environ. Impact*, 1–35 (2003).
7. T. E. Cropper, E. Hanna, An analysis of the climate of Macaronesia, 1865–2012. *Int. J. Climatol.* **34**, 604–622 (2014).
8. A. Hernández, *et al.*, A 2,000-year Bayesian NAO reconstruction from the Iberian Peninsula. *Sci. Rep.* **10**, 14961 (2020).
9. S. E. Connor, *et al.*, The ecological impact of oceanic island colonization – a palaeoecological perspective from the Azores. *J. Biogeogr.*, 1–17 (2012).
10. J. F. N. van Leeuwen, *et al.*, Native or introduced? Fossil pollen and spores may say. An example from the Azores Island. *Neobiota* **6**, 27–34 (2005).
11. C. A. Góis-Marques, *et al.*, The Loss of a Unique Palaeobotanical Site in Terceira Island Within the Azores UNESCO Global Geopark (Portugal). *Geoheritage* **11**, 1817–1825 (2019).
12. C. A. Góis-Marques, L. de Nascimento, M. Menezes de Sequeira, J. M. Fernández-Palacios, J. Madeira, The Quaternary plant fossil record from the volcanic Azores Archipelago (Portugal, North Atlantic Ocean): a review. *Hist. Biol.* **31**, 1267–1283 (2019).
13. J. M. Moreira, *Alguns aspectos de intervenção humana na evolução da paisagem da ilha de S. Miguel (Açores)* (Serviço Nacional de Parques, Reservas e Conservação da Natureza, 1987).
14. G. Frutuoso, *Livro Sexto das Saudades da Terra*, Instituto (1978).
15. R. D. Gregório, “Terra e fortuna nos primórdios da Ilha Terceira (1450-1550),” Universidade dos Açores. (2006).
16. G. Frutuoso, *Livro Quarto das Saudades da Terra* (Instituto Cultural de Ponta Delgada, 1981).
17. K. A. Triantis, *et al.*, Extinction debt on oceanic Islands. *Ecography* **33**, 285–294 (2010).
18. R. B. Elias, *et al.*, Natural zonal vegetation of the Azores Islands: Characterization and potential distribution. *Phytocoenologia* **46**, 107–123 (2016).
19. J. Porteiro, “Lagoas dos Açores: elementos de suporte ao planeamento integrado,” Universidade dos Açores, Ponta Delgada. (2000).
20. C. L. Pereira, *et al.*, Biogeography and lake morphometry drive diatom and chironomid assemblages’ composition in lacustrine surface sediments of oceanic islands.

Hydrobiologia **730**, 93–112 (2014).

21. V. Gonçalves, “Contribuição do estudo das microalgas para a avaliação da qualidade ecológica das lagoas dos Açores: fitoplâncton e diatomáceas bentónicas,” University of the Azores, Ponta Delgada. (2008).
22. J. V. Cruz, *et al.*, Sete Cidades and Furnas lake eutrophication (São Miguel, Azores): Analysis of long-term monitoring data and remediation measures. *Sci. Total Environ.* **520**, 168–186 (2015).
23. A. C. Costa, *et al.*, Non-indigenous and Invasive Freshwater Species on the Atlantic Islands of the Azores Archipelago. *Front. Ecol. Evol.* **9**, 211 (2021).
24. M. G. Matias, *et al.*, Divergent trophic responses to biogeographic and environmental gradients. *Oikos* **126**, 101–110 (2017).
25. P. M. Raposeiro, A. M. Cruz, S. J. Hughes, A. C. Costa, Azorean freshwater invertebrates: Status, threats and biogeographic notes. *Limnetica* **31**, 13–22 (2012).
26. P. M. Raposeiro, A. Sáez, S. Giral, A. C. Costa, V. Gonçalves, Causes of spatial distribution of subfossil diatom and chironomid assemblages in surface sediments of a remote deep island lake. *Hydrobiologia* **815**, 141–163 (2018).
27. M. R. Talbot, “Nitrogen isotopes in paleolimnology” in *Tracking Environmental Change Using Lake Sediments. Physical and Geochemical Methods*, J. P. Smol, H. J. B. Birks, W. M. Last, Eds. (Kluwer Academic Publishers, 2001), pp. 401–439.
28. K. D. Bennett, W. J. Willis, “Pollen” in *Tracking Environmental Change Using Lake Sediments, Terrestrial, Algal and Siliceous Indicators*, J. P. Smol, H. J. B. Birks, W. M. Last, Eds. (Kluwer, 2001), pp. 5–32.
29. R. B. Moore, *Geology of the three Late Quaternary Stratovolcanoes on São Miguel, Azores* (US Geological Survey Bulletin, 1991).
30. M. Reille, *Pollen et Spores d’Europe et d’Afrique du Nord* (Laboratoire de Botanique Historique et Palynologie).
31. D. Demske, P. E. Tarasov, T. Nakagawa, S. P. Members, Atlas of pollen, spores and further non-pollen palynomorphs recorded in the glacial-interglacial la Quaternary sediments of lake Suigetsu, central Japan. *Quat. Int.* **290–291**, 164–238 (2013).
32. B. van Geel, A. Aptroot, Fossil ascomycetes in Quaternary deposits. *Nov. Hedwigia* **82**, 313–329 (2006).
33. B. van Geel, *et al.*, Diversity and ecology of tropical African fungal spores from a 25,000-year palaeoenvironmental record in southeastern Kenya. *Rev. Palaeobot. Palynol.* **164**, 174–190 (2011).
34. C. Cugny, F. Mazier, D. Galop, Modern and fossil non-pollen palynomorphs from the Basque mountains (western Pyrenees, France): the use of coprophilous fungi to reconstruct pastoral activity. *Veg. Hist. Archaeobot.* **19**, 391–408 (2010).
35. E. Montoya, V. Rull, T. Vegas-Vilarrúbia, Non-pollen palynomorph studies in the Neotropics: the case of Venezuela. *Rev. Palaeobot. Palynol.* **186**, 102–130 (2012).
36. C. Joly, L. Barillé, M. Barreau, A. Mancheron, L. Visset, Grain and annulus diameter as criteria for distinguishing pollen grains of cereals from wild grasses. *Rev. Palaeobot. Palynol.* **146**, 221–233 (2007).
37. H.-J. Beug, *Leitfaden der Pollesbestimmung für Mitteleuropa und angrenzende Gebiete* (2004).
38. V. Rull, A note on pollen counting in palaeoecology. *Pollen Spores* **29**, 471–480 (1987).
39. V. Rull, *et al.*, Vegetation and landscape dynamics under natural and anthropogenic

- forcing on the Azores Islands: A 700-year pollen record from the São Miguel Island. *Quat. Sci. Rev.* **159**, 155–168 (2017).
40. G. Berggren, *Atlas of seeds. Part 2. Cyperaceae* (Swedish Museum of Natural History, 1964).
 41. G. Berggren, *Atlas of seeds. Part 3. Salicaceae-Cruciferae* (Swedish Museum of Natural History, 1981).
 42. W. Beijerinck, *Zadenatlas der Nederlandsche flora:: ten behoeve van de botanie, palaeontologie, bodemcultuur en warenkennis* (Backhuys & Meesters, 1976).
 43. G. Grosse-Brauckmann, Über pflanzliche Makrofossilien mitteleuropäischer Torfe. II. Weitere Reste (Früchte und Samen, Moose u.a.) und ihre Bestimmungsmöglichkeiten. *Telma* **4**, 51–117 (1974).
 44. G. Grosse-Brauckmann, B. Streit, Pflanzliche Makrofossilien mitteleuropäischer Torfe. III. Früchte, Samen und einige Gewebe (Fotos von fossilen Pflanzenresten). *Telma* **22**, 53–102 (1992).
 45. G. Grosse-Brauckmann, Über pflanzliche Makrofossilien mitteleuropäischer Torfe. I. Gewebereste krautiger Pflanzen und ihre Merkmale. *Telma* **2**, 19–55 (1972).
 46. D. Mauquoy, B. Hughes PDM van Geel, A protocol for plant macrofossil analysis of peat deposits. *Mires Peat* **7**, 1–5 (2010).
 47. I. Renberg, A procedure for preparing large sets of diatom slides from sediment cores. *J. Paleolimnol.* **4**, 87–90 (1990).
 48. K. Krammer, H. Lange-Bertalot, *Bacillariophyceae. 2/5: English and French translation of the keys*, H. Ettl, Ed. (G. Fisher Verlag, 2000).
 49. K. Krammer, H. Lange-Bertalot, *Bacillariophyceae*.
 50. K. Krammer, H. Lange-Bertalot, *Bacillariophyceae. 2/3: Centrales, Fragilariaceae, Eunotiaceae*, H. Ettl, Ed. (G. Fisher Verlag, 1991).
 51. K. Krammer, H. Lange-Bertalot, *Bacillariophyceae. 2/4: Achnantheaceae*, H. Ettl, Ed. (G. Fisher Verlag, 1991).
 52. K. Krammer, H. Lange-Bertalot, *Bacillariophyceae 2/2 Bacillariaceae, Epithemiaceae, Surirellaceae.*, H. Ettl, Ed. (G. Fisher Verlag, 1988).
 53. H. Lange-Bertalot, *Diatoms of the European Inland Waters and comparable Habitats*.
 54. J. Prygiel, M. Coste, *Guide Méthodologique pour la mise en oeuvre de l'Indice Biologique Diatomées* (Agences de l'Eau, 2000).
 55. V. Gonçalves, H. Marques, A. Fonseca, “Lista das Diatomáceas (Bacillariophyta)” in *Listagem Dos Organismos Terrestres e Marinhos Dos Açores*, P. A. V Borges, et al., Eds. (Principia, 2010), pp. 81–97.
 56. J. A. Wolin, J. R. Stone, “Diatoms as indicators of water-level change in freshwater lakes” in *The Diatoms Applications to Environmental and Earth Sciences*, E. F. Stoermer, J. P. Smol, Eds. (Cambridge University Press, 2010), pp. 174–185.
 57. J. R. Johansen, “Diatoms of aerial habitats” in *The Diatoms Applications to Environmental and Earth Sciences*, E. F. Stoermer, J. P. Smol, Eds. (Cambridge University Press, 2010), pp. 465–472.
 58. S. J. Brooks, P. G. Langdon, O. Heiri, *The Identification and Use of Palaeartic Chironomidae Larvae in Palaeoecology* (Quaternary Research Association, 2007).
 59. S. R. Q. Serra, M. A. S. Graça, S. Dolédec, M. J. Feio, Discriminating permanent from temporary rivers with traits of chironomid genera. *Int. J. Limnol.* **53**, 161–174 (2017).

60. V. Rull, N. D. Stansell, E. Montoya, M. Bezada, M. B. Abbott, Palynological signal of the Younger Dryas in the tropical Venezuelan andes. *Quat. Sci. Rev.* **29**, 3045–3056 (2010).
61. P. J. Reimer, *et al.*, The IntCal13 Northern Hemisphere radiocarbon age calibration curve (0-55 cal kBP. *Radiocarbon* **62**, 725–757 (2020).
62. J. A. Sanchez-Cabeza, P. Masqué, I. Ani-Ragolta, Lead-210 and Po-210 analysis in sediments and soils by microwave acid digestion. *J. Radioanal. Nucl. Chem.* **227**, 19–22 (1998).
63. A. C. Ruiz-Fernández, C. Hillaire-Marcel, ^{210}Pb -derived ages for the reconstruction of terrestrial contaminant history into the Mexican Pacific coast: Potential and limitations. *Mar. Pollut. Bull.* **59**, 134–145 (2009).
64. W. W. Flynn, The determination of low levels of polonium-210 in environmental materials. *Anal. Chim. Acta* **43**, 221–227 (1968).
65. P. G. Appleby, F. Oldfield, The calculation of lead-210 dates assuming a constant rate of supply of unsupported ^{210}Pb to the sediment. *Catena*, 1–8 (1978).
66. J. A. Sanchez-Cabeza, A. C. Ruiz-Fernández, ^{210}Pb sediment radiochronology: an integrated formulation and classification of dating models. *Geochim. Cosmochim. Acta* **82**, 183–200 (2012).
67. J. A. Robbins, “Geochemical and geophysical applications of radioactive lead” in *The Biogeochemistry of Lead in the Environment*, J. O. Nriagu, Ed. (Elsevier, 1978), pp. 285–393.
68. J. A. Sanchez-Cabeza, A. C. Ruiz-Fernández, J. F. Ontiveros-Cuadras, L. H. P. Bernal, C. Olid, Monte Carlo uncertainty calculation of ^{210}Pb chronologies and accumulation rates of sediments and peat bogs. *Quat. Geochronol.* **23**, 80–93 (2014).
69. M. Blaauw, J. A. Christen, J. E. Vazquez, S. Goring, Clam - Classical Age-Depth Modelling of Cores from Deposits. *R Packag. version 2.3.7* (2020).
70. M. Blaauw, Methods and code for “classical” age-modelling of radiocarbon sequences. *Quat. Geochronol.* **5**, 512–518 (2010).
71. N. J. Abram, *et al.*, Early onset of industrial-era warming across the oceans and continents. *Nature* **536**, 411–418 (2016).
72. Q. Fu, L. Lin, J. Huang, S. Feng, A. Gettelman, Changes in terrestrial aridity for the period 850–2080 from the Community Earth System Model. *J. Geophys. Res. Atmos.* **121**, 2857–2873 (2016).
73. C. C. Raible, *et al.*, Tambora 1815 as a test case for high impact volcanic eruptions: Earth system effects. *WIREs Clim. Chang.* **7**, 569–589 (2016).
74. P. M. Sousa, *et al.*, North Atlantic integrated water vapor transport from 850 to 2100 CE: Impacts on Western European rainfall. *J. Clim.* **33**, 263–279 (2020).
75. R. Zhang, *et al.*, A Review of the Role of the Atlantic Meridional Overturning Circulation in Atlantic Multidecadal Variability and Associated Climate Impacts. *Rev. Geophys.* **57**, 316–375 (2019).
76. M. P. King, E. Yu, J. Sillmann, Impact of strong and extreme El Niños on European hydroclimate. *Tellus A Dyn. Meteorol. Oceanogr.* **72**, 1–10 (2020).
77. T. J. Osborn, K. R. Briffa, S. F. B. Tett, P. D. Jones, R. M. Trigo, Evaluation of the North Atlantic Oscillation as simulated by a coupled climate model. *Clim. Dyn.* **15**, 685–702 (1999).
78. L. Comas-Bru, A. Hernández, Reconciling North Atlantic climate modes: revised monthly indices for the East Atlantic and the Scandinavian patterns beyond the 20th century. *Earth*

- Syst. Sci. Data* **10**, 2329–2344 (2018).
79. D. Vázquez-Loureiro, *et al.*, Diatom-inferred ecological responses of an oceanic lake system to volcanism and anthropogenic perturbations since 1290 CE. *Palaeogeogr. Palaeoclimatol. Palaeoecol.* **534**, 109285 (2019).
 80. R Core Team, R: A Language and Environment for Statistical Computing (2020).
 81. P. A. Meyers, Applications of organic geochemistry to paleolimnological reconstructions: a summary of examples from the Laurentian Great Lakes. *Org. Geochem.* **34**, 261–289 (2003).
 82. P. A. Meyers, Preservation of elemental and isotopic source identification of sedimentary organic matter. *Chem. Geol.* **114**, 289–302 (1994).
 83. P. M. Raposeiro, *et al.*, Impact of the historical introduction of exotic fishes on the chironomid community of Lake Azul (Azores Islands). *Palaeogeogr. Palaeoecol.* **466**, 77–88 (2017).
 84. H. Van Dam, A. Mertens, J. Sinkeldam, A coded checklist and ecological indicator values of freshwater diatoms from The Netherlands. *Netherl. J. Aquat. Ecol.* **28**, 117–133 (1994).
 85. S. Naeher, A. Gilli, R. P. North, Y. Hamann, C. J. Schubert, Tracing bottom water oxygenation with sedimentary Mn/Fe ratios in Lake Zurich, Switzerland. *Chem. Geol.* **352**, 125–133 (2013).
 86. M. E. Mann, *et al.*, Global signatures and dynamical origins of the Little Ice Age and Medieval Climate Anomaly. *Science* **326**, 1256–1260 (2009).